ACS OMEGA

Open Access

http://pubs.acs.org/journal/acsodf

Article

Regorafenib Attenuates Osteoclasts Differentiation by Inhibiting the NF-κB, NFAT, ERK, and p38 Signaling Pathways

Lin Zhou,[‖] Peiru Su,[‖] Xiangya Luo, Xuanli Zhong, Qian Liu, Yuangang Su, Chunping Zeng,* and Ge Li*

Cite This: *ACS Omega* 2024, 9, 33574−33593

Read Online

ACCESS | Metrics & More | Article Recommendations | Supporting Information

ABSTRACT: Osteolytic diseases such as osteoporosis and neoplastic bone metastases are caused by the excessive activation of osteoclasts. Inhibiting the excessive activation of osteoclasts is a crucial strategy for treating osteolytic diseases. This study investigated the roles and mechanisms of regorafenib, a tyrosine kinase inhibitor, on osteoclasts and osteolytic diseases. We first identified the potential targets and mechanisms of regorafenib on osteoclast-related osteolytic diseases using network pharmacological analysis and molecular docking techniques. Then, we verified its role and mechanism on osteoclasts via cellular and animal experiments. Network pharmacology analysis identified 89 common targets shared by regorafenib and osteoclast-related osteolytic diseases. Enrichment analysis suggested that regorafenib may act on osteoclast-related osteolytic diseases by modulating targets such as AKT1, CASP3, MMP9, and MAPK3, regulating biological processes such as cell proliferation, apoptosis, and phosphorylation regulation, and influencing signaling pathways such as MAPK, PI3K/AKT, and osteoclast differentiation. The molecular docking results indicated that regorafenib and AKT1, CASP3, MMP9, MAPK3, and MAPK14 were stably docked. Cell experiments demonstrated that regorafenib significantly inhibited osteoclast differentiation and bone resorption in RAW 264.7 cells and bone marrow macrophages in a dose-dependent manner, with up to 50% reduction at 800 nM concentration without exhibiting cytotoxic effects. Furthermore, Western blot and RT-qPCR results demonstrated that regorafenib inhibited osteoclast differentiation by blocking the transduction of RANKL-induced NF-κB, p38, ERK, and NFAT signaling pathways. In vivo studies using an ovariectomized mouse model showed that regorafenib significantly improved bone volume fraction (BV/TV), bone surface to total volume (BS/TV), and number of trabeculae (TB.N), as well as reduced trabecular separation (Tb.Sp) compared to the OVX groups ($P < 0.05$). TRAcP staining results revealed a reduction in the number of osteoclasts with regorafenib treatment ($P < 0.01$). These results indicate that regorafenib exerts its protective effects against osteoclast-related osteolytic disease by inhibiting the RANKL-induced NF-κB, NFAT, ERK, and p38 signaling pathways. This study proves that regorafenib may serve as a potential therapeutic agent for osteoclast-related osteolytic diseases.

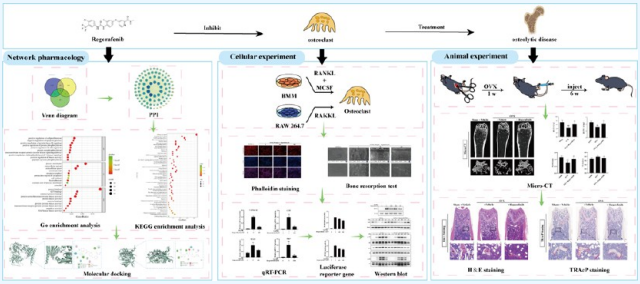

1. INTRODUCTION

Bone tissue is indispensable for providing structural support and facilitating movement within the human body.[1] Moreover, it sustains its dynamic stability through a continuous process of bone remodeling. This process involves osteoclasts breaking down old bone tissue and osteoblasts forming new bone.[2] Under normal circumstances, a balance between osteoclasts and osteoblasts ensures bone tissue's ongoing renewal and repair. However, pathological conditions such as inflammation or cancer can disrupt this equilibrium, leading to an acceleration in the activation of osteoclasts. This disruption in bone homeostasis and pathological bone resorption results in osteolytic diseases characterized by bone loss and destruction, such as osteoporosis[3] and neoplastic bone metastases.[4] Postmenopausal osteoporosis, a prevalent form of osteoporosis, primarily results from a reduction in estrogen after menopause, leading to decreased bone mass, bone structural deterioration, and pathological fractures.[5] Neoplastic bone metastases, often a complication in advanced cancer stages, mainly cause bone resorption and pathological fractures.[6] Pathological fractures, a significant complication of osteolytic diseases, not only lead to high disability and mortality rates but also impose considerable economic burdens on patients, families, and society.[7,8] As a result, addressing the treatment of osteolytic diseases and preventing fractures are critical focuses in current medical research and practice.

Drugs that inhibit bone resorption are commonly employed in treating osteolytic diseases as a therapeutic strategy.[6,9] While these drugs have shown effectiveness in clinics, their application is often hampered by their limited efficacy and

Received: February 9, 2024
Revised: June 30, 2024
Accepted: July 2, 2024
Published: July 23, 2024

various side effects. For example, alendronate and zoledronic acid, while effective in reducing osteoclastic activity,[10] can cause gastrointestinal irritation and atypical femur fracture with long-term application.[11] Denosumab, a receptor activator of nuclear factor-κB ligand (RANKL) inhibitor, specifically inhibits osteoclastogenesis and activity.[12] However, it does not significantly improve disease progression or survival following bone metastases.[13] Consequently, there is an urgent need to explore alternative drugs to treat osteolytic diseases more effectively. This need has driven our study to identify and test alternative therapeutic options that could more effectively counteract osteolytic diseases.

Recognizing the limitations of current therapies, researchers have explored additional strategies to inhibit osteoclast function. Numerous studies have highlighted the viability of targeting the pathological process of osteoclastogenesis as a therapeutic strategy for osteolytic diseases. For instance, Tao Yang et al. demonstrated that inhibiting osteoclast function could substantially reduce bone loss in models of postmenopausal osteoporosis, suggesting potential therapeutic avenues.[14] Additionally, De Leon-Oliva et al. found that targeting molecular pathways involved in osteoclast differentiation, such as the RANK/RANKL pathway, offers promising results for mitigating bone degradation in cancer-induced osteolysis.[15] Osteoclasts, multinucleated cells derived from the myeloid lineage, play a pivotal role in bone remodeling by facilitating bone resorption and breakdown through the secretion of acids and proteases.[16] The RANKL/RANK system is crucial in the regulation of osteoclast differentiation, maturation, and bone resorption activities. In the presence of macrophage-colony stimulating factor (M-CSF), RANKL binds to the receptor activator of nuclear factor-κB (RANK), activating multiple signaling pathways, including NF-κB, MAPK, etc. These pathways subsequently activate the nuclear transcription factor NFATc1, which further encourages the expression of nuclear translocation and enhances the induction of osteoclast-specific genes like V-ATPase-d2, Cathepsin K, and tartrate-resistant acid phosphatase (TRAcP).[4,17] Many compounds have been gradually shown to inhibit osteoclast differentiation and improve bone loss via regulating RANKL-induced signaling pathway, such as antidepressant duloxetine hydrochloride,[18] antifungal agent ciclopirox.[19] Therefore, targeting the RANK/RANKL signaling pathway to inhibit osteoclast formation is essential for treating osteolytic diseases.

Considering the significant resources required for developing new drugs, repurposing Food and Drug Administration-approved drugs to address unmet clinical needs in osteolytic diseases presents an optimal strategy. Regorafenib (BAY 73−4506) is a multitargeted tyrosine kinase inhibitor. Preclinical studies have illustrated that regorafenib targets many kinases implicated in tumor angiogenesis, proliferation, regulation of the tumor microenvironment, and metastasis. Numerous clinical trials have demonstrated that regorafenib has broad antitumor activity, particularly in the treatment of gastrointestinal stromal tumors, metastatic colorectal cancer, and unresectable hepatocellular carcinoma.[20−22] And it received its approval from the FDA in 2012. Intriguingly, research by Iris Breitkreutz and colleagues[23] demonstrated that regorafenib could inhibit the proliferation and survival of multiple myeloma cells and prevent the differentiation of peripheral blood mononuclear cells from patients with multiple myeloma into osteoclasts in vitro. Additionally, regorafenib has been shown to disrupt tumor immunity and reduce tumor-infiltrating macrophages by inhibiting the colony-stimulating factor 1 receptor (CSF1R),[24−26] which also plays a significant role in osteoclast survival, function, and differentiation.[27,28] These findings suggest a potential role for regorafenib in treating osteolytic diseases by affecting osteoclast activity. However, the roles and mechanisms of regorafenib on osteoclastogenesis and osteolytic diseases require further investigation, as previous results were unclear.

Therefore, the primary aim of this study is to elucidate the roles and mechanisms of regorafenib on osteoclastogenesis and osteolytic diseases. Significantly, this research innovatively introduces a novel application for regorafenib in treating bone diseases beyond its established use in oncology. Our study initially identified the potential targets and mechanisms of regorafenib on osteoclast-related osteolytic diseases using network pharmacological analysis and molecular docking techniques, and then assessed its role and mechanism on osteoclasts through in vitro cellular experiments. Moreover, an ovariectomized mouse model was utilized to examine its efficacy in estrogen deficiency-induced bone loss in vivo. This study provides a solid theoretical basis for further investigation and clinical application of regorafenib in the treatment of osteolytic diseases. By elucidating the pathways and targets through which regorafenib modulates osteoclast activity, we can contribute to a more targeted approach in osteolytic disease treatment, potentially improving patient quality of life and outcomes. Although our research is still preliminary, as we continue to delve deeper into these pathways, the development of multitarget drugs like regorafenib that can act on both cancer cells and bone metabolism could significantly impact the treatment of osteolytic diseases.

2. MATERIALS AND METHODS

2.1. Network Pharmacology Data Sources.

2.1.1. Screening Potential Targets of Regorafenib and Osteoclast-Related Osteolytic Diseases. According to the chemical name "regorafenib" and the CAS number "755037-03-7", the structural formula was obtained by searching the PubChem database[29] (https://pubchem.ncbi.nlm.nih.gov/). Subsequently, related targets for regorafenib were identified from the Swiss Target Prediction database,[30] the PharmMapper database (http://www.lilab-ecust.cn/pharmmapper/), and the Comparative Toxicogenomics Database[31] (CTD, https://ctdbase.org/). Finally, gene names were normalized based on the species "*Homo sapiens*" in the UniProt database[32] (https://www.uniprot.org/). After deduplication and sorting, the data were finally stored in Excel as regorafenib-related targets.

Separately using "osteolytic disease" and "osteoclasts" as keywords, the genes associated with osteolytic disease and osteoclasts were extracted from three databases: GeneCards[33] (https://www.genecards.org/), the Online Mendelian Inheritance in Man[34] (OMIM) database (https://www.omim.org/), and the PharmGKB database[35] (https://www.pharmgkb.org/), and using species "*H. sapiens*" as the screening condition. After deduplication, the data were ultimately receptively compiled and stored in Excel as osteolytic disease targets and osteoclast targets.

The targets of regorafenib, osteolytic disease, and osteoclast were respectively imported into the online Web site (https://bioinfogp.cnb.csic.es/tools/venny/) to construct a Venn diagram.[36] The common intersecting targets across all three

https://doi.org/10.1021/acsomega.4c01308
ACS Omega 2024, 9, 33574−33593

groups were identified as potential targets of regorafenib for treating osteoclast-related osteolytic diseases.

2.1.2. Constructing the Protein−Protein Interaction Networks. The common targets were then processed using the STRING database[37] (https://string-db.org/) to create a Protein−protein interaction (PPI) diagram with species the "*H. sapiens*" as the screening condition. The PPI diagram was subsequently next exported in. tsv format, which was further visually processed and analyzed utilizing Cytoscape software[38] (v.3.9.1). Topological analysis was carried out using the CytoHubba plugin in Cytoscape software (v.3.9.1), based on Maximal Neighborhood Component (MNC) algorithm,[39] to identify key targets.

2.1.3. GO Enrichment and KEGG Analysis. To explore the potential biological functions and major signaling pathways of regorafenib in treating osteoclast-related osteolytic diseases, gene ontology (GO) and kyoto encyclopedia of genes and genomes (KEGG) enrichment analyses[40] were separately conducted on the potential targets obtained from Section 2.1.1 using the DAVID databases[41] (https://david.ncifcrf.gov/tools.jsp). Lastly, the results from these analyses were visually processed using the bioinformatics online platform (http://www.bioinformatics.com.cn/).

2.1.4. Molecular Docking. Based on the outcomes of the bioinformatics analysis, key targets, including AKT1, CASP3, MMP9, MAPK3, and MAPK14, were selected for executing molecular docking with regorafenib. Regorafenib was chosen as the ligand and imported into Chem3D software to undergo energy minimization. Each key target served as the receptor, which was imported into the UniProt database (https://www.uniprot.org/) to download associated protein files in .pdb format. These files were imported into PyMOL software to remove water molecules and small molecule components and then imported into AutoDock Tools hydrogenation. Molecular docking and visualization analyses were carried out leveraging PyMOL software.[42] The docking effect of each key target and regorafenib was evaluated using the binding energy.

2.2. Experimental Verification. *2.2.1. Chemicals and Reagents.* Regorafenib (CAS No. 755037-03-7) was purchased from MedChemExpress Company (Shanghai, China) and stored at −20 °C after being dissolved in DMSO as a 10 mM stock solution. And regorafenib was then diluted to the target concentration with culture medium before use.[43] Fetal bovine serum (FBS) and α-modified minimal essential medium (α-MEM) were acquired from Gibco (Massachusetts). The cell counting kit-8 (CCK-8) was acquired from Bestbio Company (Shanghai, China). RANKL was purchased from R&D Systems (Minneapolis). Anti-NFATc1 antibodies were purchased from Santa Cruz Biotechnology (Dallas). Anti-IκB-α and anti-β-actin antibodies were purchased from Zen Bioscience (Chengdu, China). Antibodies to phosphorylated p38, p38, phosphorylated JNK, JNK, phosphorylated ERK, and ERK were ordered from Cell Signaling Technology (Beverly). M-CSF was purchased from Detai Bioscience (Nanjing, China). Bicinchoninic acid (BCA) protein detection kit and tartrate-resistant acid phosphatase (TRAcP) staining solutions were purchased from Sigma (USA). The RNA extraction kit was purchased from Yishan Biotechnology Company (Shanghai, China). Phalloidin and DAPI staining solutions were purchased from Solarbio (Beijing, China). The luciferase assay kit was purchased from Promega (Wisconsin).

2.2.2. Ethical Statement. The extraction of bone marrow-derived macrophages (BMMs) and all animal experiments were approved by the Jinan University Laboratory Animal Welfare and Ethical Committee (No. 20230303-0055). All animals were procured from Zhuhai Baishitong Biotechnology Company, with the certification number SCXK2020-0051.

2.2.3. In Vitro Induction of Osteoclast Differentiation and Identification. RAW 264.7 cells were cultured in 100 mm cell culture dishes with α-MEM complete culture medium (supplemented with 10% fetal bovine serum (FBS)). Once the logarithmic phase of RAW 264.7 cells had been attained, the cells were seeded onto a 96-well plate at a density of 1.5×10^3/well and incubated with α-MEM complete culture medium overnight. The following day, RAW 264.7 cells were cultured with α-MEM complete culture medium containing RANKL[44] (50 ng/mL) and varying concentrations of regorafenib (0, 100, 200, 400, 800 nM).

Freshly extracted BMMs from 4-week-old C57BL/6J mice were cultured in T75 culture flasks, utilizing α-MEM complete culture medium that contained 100 ng/mL M-CSF for a period of 6−7 days,[36] with the culture medium refreshed every 2 days. When the density of BMMs reached 80% or more, the cells were inoculated onto a 96-well plate at a density of 6×10^3/well and incubated with α-MEM complete culture medium that contained 100 ng/mL M-CSF. The next day, BMMs were cultured with α-MEM complete culture medium containing RANKL (50 ng/mL) and 100 ng/mL M-CSF, with concentrations of regorafenib ranging from 0 to 800 nM. The culture medium for RAW 264.7 cells and BMMs was refreshed every 2 days until multinucleated osteoclasts formed (approximately 5 days). At the end of the experiment, the cells were fixed using 4% paraformaldehyde (PFA) for 20 min and then stained with TRAcP staining solutions for 30 min. TRAcP-positive cells possessing more than three nuclei were identified and quantified under a DMI6000B inverted microscope (Leica, Germany).

2.2.4. CCK8 Assay for Cell Viability. Cell viability was evaluated using a CCK-8 assay Kit. BMMs and RAW 264.7 cells were respectively inoculated onto 96-well culture plates at a density of 1.5×10^4/well using α-MEM complete culture medium overnight. The next day, the culture medium in each well was replaced with α-MEM complete medium containing different concentrations of regorafenib (0, 100, 200, 400, and 800 nM). After incubating the 96-well culture plates at 37 °C in a 5% CO_2 incubator for 48 h, 10 μL of CCK-8 solution was added to each well, following the manufacturer's instructions, and then incubated for 2 h. The absorbance of each well was measured using an Epoch2 microplate spectrophotometer at a wavelength of 450 nm. Finally, cell viability was calculated to evaluate the effect of regorafenib on BMMs and RAW 264.7 cells.

2.2.5. Detection of F-Actin Ring with Phalloidin Staining. To evaluate the impact of regorafenib on the structure of the F-actin ring in osteoclasts, BMMs were seeded onto a 96-well plate at a density of 6×10^3/well and incubated overnight with α-MEM complete medium containing M-CSF (100 ng/mL). The following day, BMMs were stimulated with M-CSF (100 ng/mL) and RANKL (50 ng/mL), along with varying concentrations of regorafenib (0, 400, and 800 nM). After 5 days, the osteoclasts were fixed using 4% PFA for 30 min. After three washes with PBS, the cells were permeabilized with 0.5% Triton X-100 for 3 min. Phalloidin staining solution was then applied to each well, followed by an incubation period of 40 min in a dark room. Subsequently, the cells were washed with PBS, and the nuclei were stained with DAPI for 3 min.

https://doi.org/10.1021/acsomega.4c01308
ACS Omega 2024, 9, 33574−33593

Observations and image capture were performed using a DMI6000B inverted fluorescence microscope (Leica, Germany).

2.2.6. Bone Resorption Experiment with Bovine Bone Slices. Bovine bone slices were utilized to assess the effect of regorafenib on bone resorption capacity. The bone slices were marked on the back with a pencil, immersed in 75% alcohol for 24 h, and then rinsed twice with deionized water. These bone slices were then placed in a 100 mL beaker, filled with 50 mL of deionized water, and autoclaved for use. BMMs were cultured on the bovine bone slices in 96-well plates at a density of 1×10^4/well, using α-MEM medium supplemented with RANKL (50 ng/mL) and M-CSF (100 ng/mL). The culture medium was changed every 2 days until small osteoclasts formed (approximately 3 days). Subsequently, the cells were treated with α-MEM medium containing RANKL (50 ng/mL) and M-CSF (100 ng/mL), along with regorafenib at concentrations of 400 and 800 nM. After 5 days of continued treatment, the bone slices were fixed using 2% glutaraldehyde for 1 h. Following that, the bone slices were carefully removed from the wells, and the cells were gently brushed off the slices. The bone resorption pits were photographed using a SUPRA55 scanning electron microscope (Zeiss, Germany). ImageJ software was employed to quantify the number of bone resorption pits.

2.2.7. Real-Time PCR Analysis of Gene Expression. The experiments described above revealed that regorafenib significantly inhibited osteoclast differentiation at a concentration of 800 nM. Therefore, this concentration was selected as the effective concentration for subsequent experiments. RAW264.7 cells were seeded onto a 6-well plate with a density of 5×10^4/well and culture with α-MEM medium supplemented with 50 ng/mL RANKL. Concurrently, cells were treated or not treated with 800 nM regorafenib for 5 days. An RNA extraction kit was utilized for RNA extraction from the cells according to the manufacturer's instructions, and this total RNA was employed to synthesize complementary DNA (cDNA) with the PrimeScript RT reagent kit (Takara, DRR037A) following the protocol. Quantitative real-time polymerase chain reaction (qRT-PCR) was performed using TB Green Premix Ex TaqII (Tli RNaseH Plus) on the 7500 Real-Time PCR System to detect amplification of osteoclast-specific genes. The PCR cycle parameters were as follows: 95 °C for 30 s, 95 °C for 40 s, and 60 °C for 34 s. The cycle was repeated 40 times. The $2^{-\Delta\Delta CT}$ method was utilized to calculate the relative expression of specific genes, with GAPDH as the internal reference. Gene-specific primers utilized for qRT-PCR amplification are listed in Table 1.

2.2.8. Luciferase Reporter Gene Detection of NF-κB and NFATc1. In order to evaluate the activities of NF-κB and NFATc1, RAW264.7 cells were stably transfected with NF-κB and NFATc1 luciferase reporter genes using the pGL4.32 [luc2P/NF-κB-RE/Hygro] and pGL4.30 [luc2P/NFAT-RE/Hygro] vectors (Promega, USA). Stably transfected cells were then selected using 500 μg/mL of hygromycin (Sigma, USA). RAW 264.7 cells, stably transfected with both NF-κB and NFATc1 luciferase reporter genes, were seeded at densities of 1.5×10^5/well and 5×10^4/well in 48-well plates, respectively. Following overnight incubation, the cells were pretreated with 800 nM regorafenib and then stimulated with 50 ng/mL RANKL for 6 and 24 h, respectively. After lysing with lysis buffer, the cell lysate was collected and centrifuged at 12 000g at 4 °C for 20 min. Then, 50 μL of cell lysate samples were transferred into a white 96-well culture plate, and then 100 μL of luciferase detection reagent was added to each well according to the luciferase reporter kit's instructions. Each group was replicated three times in the experiments. Finally, the luciferase activities of NF-κB and NFATc1 were detected by the GloMax Navigator luminescence detector.

Table 1. Sequences of Gene Primers for qRT-PCR Amplification

gene	primer sequence	product length (bp)
V-ATPase d2	forward: 5′-CCTTTGTTTGACGCTGTCGG-3′	96
	reverse: 5′-CCTGTTGAATGCCAGCACAT-3′	
Cathepsin K	forward: 5′-TGTGGTTCCTGTTGGGCTTT-3′	164
	reverse: 5′-TGCACGTATTGGAAGGCAGT-3′	
TRAcP	forward: 5′-GTGGAAGCCTCTGGAAAATC-3′	106
	reverse: 5′-CTCCTCCCTCACACCCGTTA-3′	
NFATc1	forward: 5′-AGTCATCGGCGGGAAGAAG-3′	273
	reverse: 5′-CCATTGGCAGGAAGGTACG-3′	
GAPDH	forward: 5′-GGCATTGTGGAAGGGCTCAT-3′	219
	reverse: 5′-GGACACATTGGGGGTAGGAAC-3′	

2.2.9. Western Blot. To evaluate the early impact of regorafenib on signaling pathways related to osteoclast activation, RAW 264.7 cells were seeded into 6-well plates at a density of 1×10^5/well. The cells were pretreated with 800 nM regorafenib and then stimulated with 50 ng/mL RANKL for various time intervals: 0, 5, 10, 20, 30, and 60 min. Additionally, to investigate the impact of varying concentrations of regorafenib on osteoclast-related signaling pathways, RAW 264.7 cells were seeded overnight in a 6-well plate at a density of 5×10^4/well. Following that, the cells were treated with 50 ng/mL RANKL and different concentrations of regorafenib (0, 200, 400, and 800 nM) for 5 days.

The total cellular proteins were lysed and extracted using the cell lysis solution, which consisted of RIPA lysis buffer, phosphatase inhibitors, and protease inhibitors mixed at a ratio of 100:1:1. The protein concentration of each sample was determined using the BCA protein detection reagent according to the instructions. Based on the measured protein concentration, the samples were adjusted to the same concentration using RIPA lysate. Subsequently, these proteins were loaded sequentially to the wells of 10% SDS-PAGE in a volume of 25 μg, separated by electrophoresis, and then transferred onto poly(vinylidene difluoride) (PVDF) membranes. After being blocked with 5% skim milk powder for 2 h, the PVDF membranes were incubated with particular primary antibodies overnight at 4 °C. The specific primary antibodies used included JNK (1:1000, #9252, CST, Beverly, USA), p-JNK (Thr183/Tyr185) (1:1000, #4668, CST), ERK (1:1000, #4695, CST), p-ERK (Thr202/Tyr204) (1:1000, #4370, CST), p38 (1:1000, #8690, CST), p-p38(Thr180/Tyr182) (1:1000, #4511, CST), IκB-α (1:5000, #383322, Zen Bioscience, Chengdu, China), β-actin (1:10 000, #380624, Zen Bioscience), and NFATc1 (1:1000, sc-7294, Santa Cruz, Dallas, USA). Following three washes with TBS containing

https://doi.org/10.1021/acsomega.4c01308
ACS Omega 2024, 9, 33574−33593

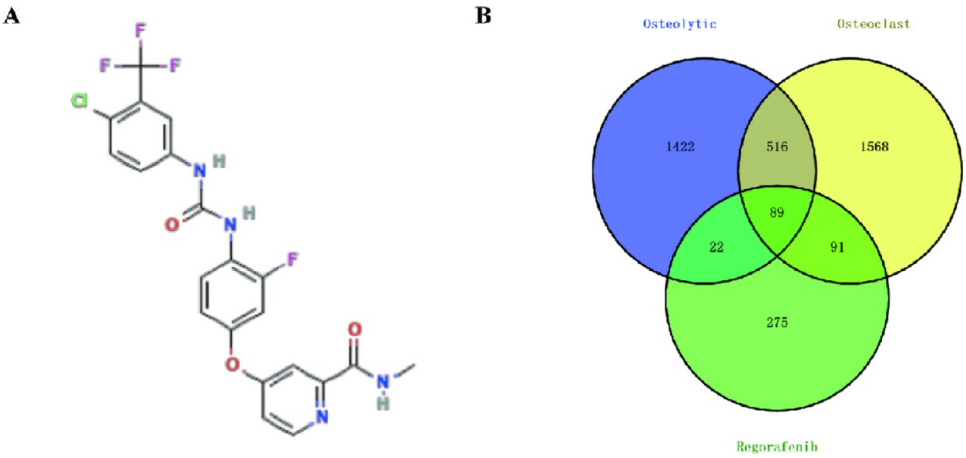

Figure 1. Potential common targets for regorafenib and osteoclast-related osteolytic diseases. (A) Molecular formula of regorafenib. (B) Venn diagram for the common intersecting targets of regorafenib and osteoclast-related osteolytic diseases.

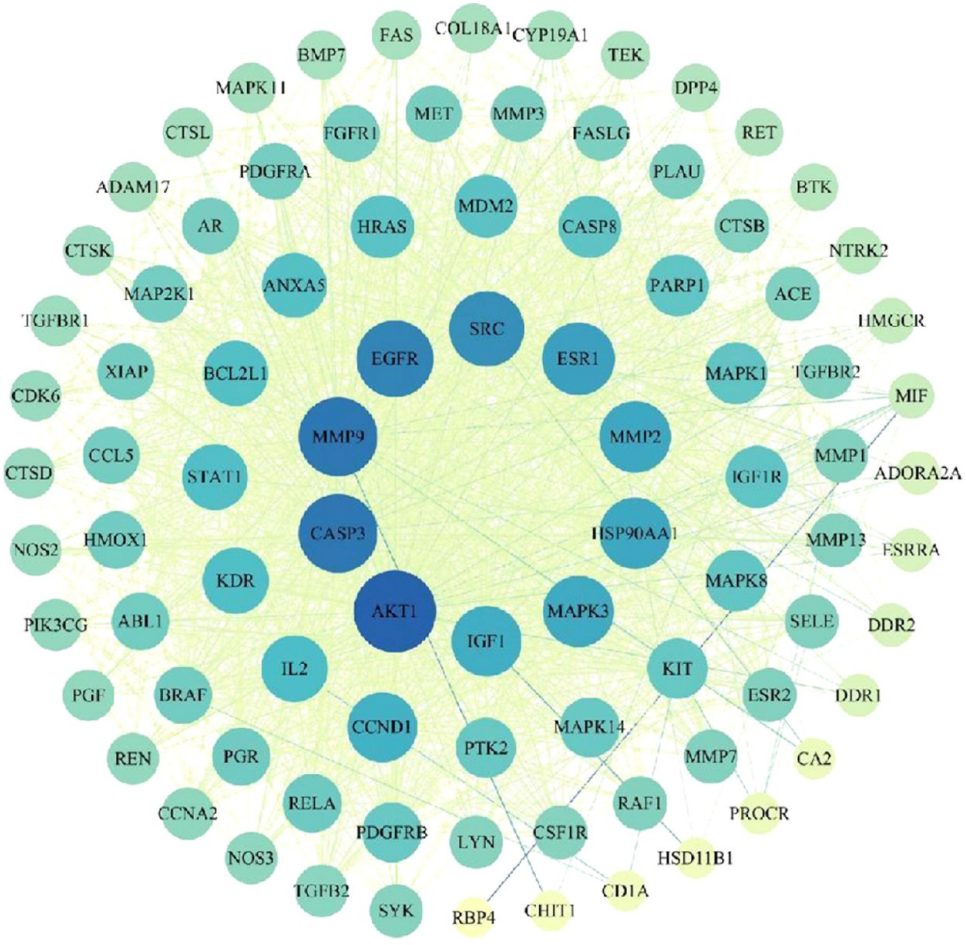

Figure 2. PPI network of potential targets for regorafenib acting on osteoclast-related osteolytic diseases. Higher degrees of correlation indicate larger node sizes, blue indicates a higher degree, and green represents a lower degree.

0.1% Tween, the membranes were incubated with corresponding HRP-conjugated secondary antibodies for 1 h. The secondary antibodies used were as follows: antirabbit IgG antibody (1:10 000; #511203; Zen Bioscience, Chengdu, China) and antimouse IgG antibody (1:10 000; #511103; Zen Bioscience). The protein bands were visualized using an enhanced chemiluminescence kit from Meilunbio (Suzhou, China), and images were captured using Bio-Rad's ChemiDoc chemiluminescence imaging system (California, USA). Finally, the quantification of the protein bands was performed using ImageJ software.

2.2.10. Construction of Ovariectomized (OVX) Mouse Model. Eighteen 10-week-old C57BL/6 female mice, each with a body mass of approximately 18 ± 2 g, were provided by Zhuhai Baishitong Biotechnology Company (No. SCXK2020-0051). All mice were randomly divided into three groups, with

https://doi.org/10.1021/acsomega.4c01308
ACS Omega 2024, 9, 33574−33593

six in each group: a Sham operation group (sham), an ovariectomized mice model group (OVX), and an ovariectomized mice model group plus10 mg/kg of regorafenib treatment group (OVX + regorafenib). The dose of regorafenib was chosen based on the literature provided by the manufacturer, which reported favorable effects of regorafenib in inhibiting tumor growth in mice.[45] After 1 week of acclimatization feeding, surgeries were carried out under tribromoethanol anesthesia. Both the OVX and the OVX + regorafenib groups underwent bilateral ovary removal in this process. In contrast, the sham-operated group, serving as a control, only had the ovaries isolated but not resected. Following a week of postoperative recovery, the mice in the OVX + regorafenib group received intraperitoneal injections of 10 mg/kg regorafenib every 2 days for a duration of 6 weeks. In contrast, the mice in the sham and OVX groups were given intraperitoneal injections of an equivalent volume of saline to serve as vehicle controls.

2.2.11. Micro-CT Analysis. A Scanco Viva CT80 micro-CT instrument was utilized to scan and image the femurs of mice from three groups (n = 6 in each group). The scanning parameters were set to a voltage of 55 kV, a current of 145 mA, and a resolution of 10.4 μm. The images were reconstructed using the SkyScan DataViewer software (SkyScan, Knotich, Belgium). Additionally, CT Analyzer (CTAn) software (Brukermicro-CT, Kontich, Belgium) was used to identify and analyze bone parameters and microstructural changes in the region of interest (ROI).[46] These bone parameters included bone volume fraction (BV/TV), bone surface to total volume (BS/TV), trabecular number (Tb.N), trabecular thickness (Tb.Th), and trabecular separation (Tb.Sp). The ROI was defined as an area of cancellous bone located 0.5 mm below and extending 1 mm in height from the growth plate.

2.2.12. Histological Analysis. The femurs were fixed in 4% PFA for more than 48 h. Subsequently, they were decalcified with EDTA for 4−6 weeks. The femurs were then dehydrated, embedded in paraffin, and sectioned into slices with a thickness of 0.5 mm. These femur sections were stained with Hematoxylin and Eosin (H&E), and TRAcP. All stained tissue sections underwent digitization using a Pannoramic MIDI digital section scanner, and the captured images were magnified with CaseViewer software (Version 2.4). Bone histomorphometry and quantification analysis of the femur sections were performed using ImageJ software.

3. STATISTICAL ANALYSIS

Data are represented as the mean ± standard deviation (SD), obtained from at least three biologically independent experiments. For statistical analysis, a one-way ANOVA accompanied by LSD-t test post hoc test for multiple comparisons or a two-tailed Student's t test for comparing two groups was utilized. A p-value of <0.05 was deemed statistically significant.

4. RESULTS

4.1. Potential Target Identification and PPI Network Analysis. The structural formula of regorafenib is presented in Figure 1A. A total of 477 potential targets of regorafenib were acquired through screening the Swiss Target Prediction, PharmMapper, and the CTD database. In addition, we obtained 2264 targets related to osteoclast and 2049 targets associated with osteolytic disease from the Genecards and OMIM databases. Finally, we obtained a total of 89 potential targets of regorafenib for treating osteoclast-related osteolytic diseases, as depicted in a Venn diagram (Figure 1B). A drug-disease PPI network was constructed using Cytoscape to illustrate the relationships among potential targets (Figure 2). Utilizing the CytoHubba plugin and based on the MNC algorithm, the top ten targets (AKT1, CASP3, MMP9, EGFR, SRC, ESR1, HSP90AA1, MMP2, MAPK3, IGF1) were identified as key targets for regorafenib in the treatment of osteoclast-associated osteolytic diseases (Table 2).

Table 2. Top Ten Targets in the PPI Network (Ranked by MNC Method)

rank	target	score
1	AKT1	79
2	CASP3	73
2	MMP9	73
4	EGFR	69
5	SRC	66
6	ESR1	61
7	MMP2	59
7	HSP90AA1	59
9	MAPK3	58
10	IGF1	57

4.2. GO Enrichment and KEGG Pathways Analysis. To further elucidate the potential mechanisms of regorafenib in treating osteoclast-related osteolytic diseases, we performed GO functional and KEGG pathway enrichment analyses on the common intersecting targets using the DAVID database. The GO enrichment analysis yielded a total of 681 results. Among these, 529 results were associated with biological processes (BPs), encompassing positive regulation of protein Kinase B signaling, cell proliferation, regulation of tyrosine kinase, regulation of phosphorylation and apoptotic process, etc. 54 results pertained to cellular components (CCs), including membrane raft, receptor complex, and extracellular region, etc. And 98 results corresponded to molecular functions (MFs), including protein tyrosine kinase activity, MAP kinase activity, ATP binding and protein binding, etc. These findings indicated that regorafenib might treat osteoclast-related osteolytic diseases by modulating these biological processes. Figure 3A shows the top 10 terms with significant MFs, BPs, and CCs enrichment.

The KEGG enrichment analysis identified a total of 156 signaling pathways that were significantly associated with the potential targets (P < 0.01). A bubble chart in Figure 3B displays the top 50 pathways. It was found that potential targets are primarily involved in signaling pathways, including cancer, MAPK, PI3K-Akt signaling, apoptosis, TNF and osteoclast differentiation, etc. Furthermore, a drug-target-pathway network for the main signaling pathways was constructed using Cytoscape software to intuitively observe the relationship between these pathways and the key targets (Figure 4).

4.3. Molecular Docking. Molecular docking was applied to validate the binding mode of the key targets with regorafenib. As per previous literature,[47] a docking score less than −5.0 suggests a stable binding affinity between the compound and its target protein. The docking score represents the binding energy between the compound and its target protein. The lower the docking score, the stronger the binding capacity between the compound molecule and its target

https://doi.org/10.1021/acsomega.4c01308
ACS Omega 2024, 9, 33574−33593

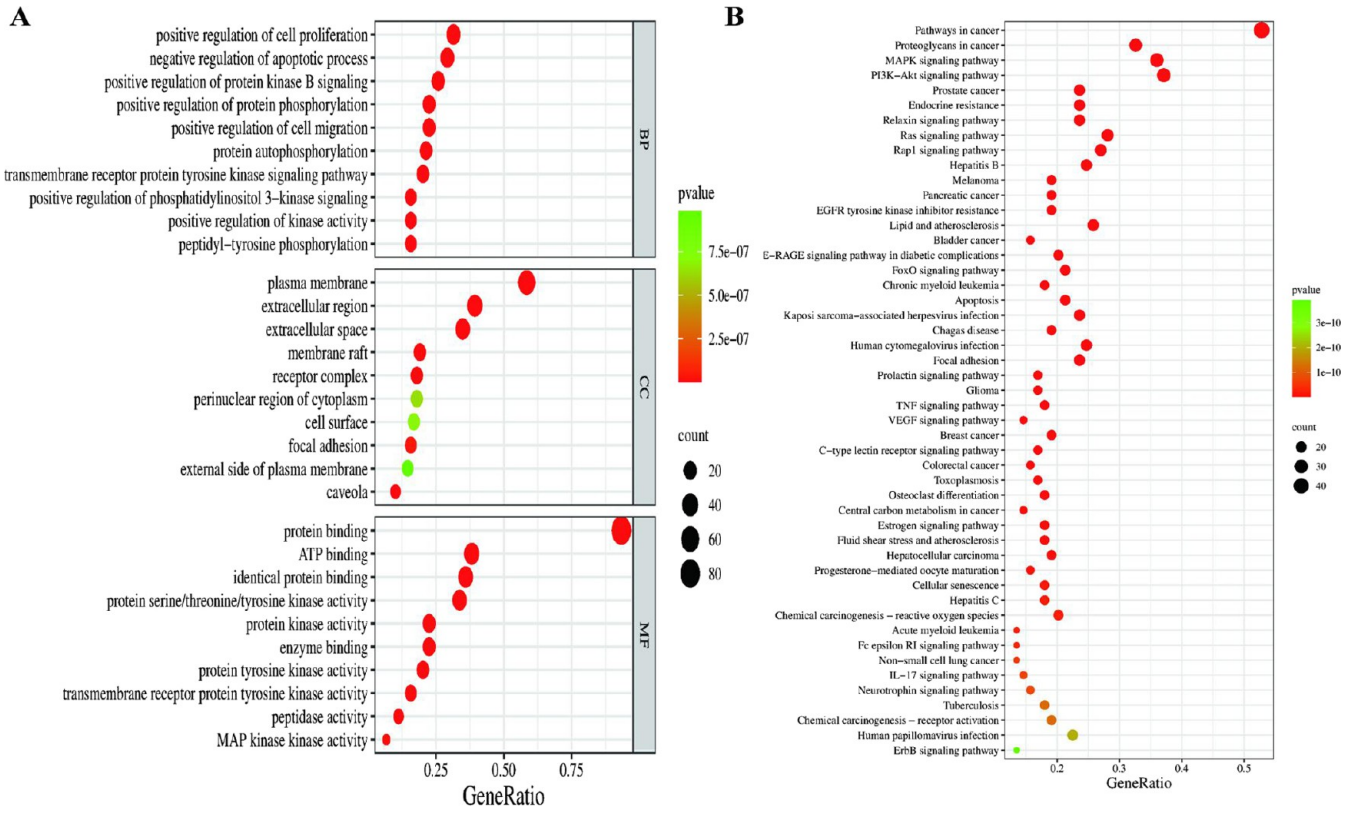

Figure 3. GO and KEGG enrichment analysis of protein targets for regorafenib acting on osteolytic diseases. (A) GO analysis of the protein targets. A bubble chart depicting the top 10 terms of BPs, CCs and MFs. (B) KEGG analysis of the protein targets. A bubble chart depicting the top 50 enriched KEGG pathways for protein targets. The size of each spot represents the number of genes, and color represents the *P* value. Larger node sizes indicate higher degrees of correlation.

protein is. Combining the results of binding energy, the molecular docking results revealed that regorafenib was stably docked with AKT1, CASP3, MMP9, MAPK3, and MAPK14 (Figure 5A−E). Notably, the binding energies between AKT1, MAPK14, MAPK3, and regorafenib were −6.8517, −6.748, and −6.4142 kcal/mol, respectively. These results suggested that regorafenib could establish strong hydrogen bonding and hydrophobic interactions with these proteins, as depicted in Figure 5F.

4.4. Regorafenib Reduced RANKL-Induced Osteoclasts In Vitro. It has been shown that low-dose regorafenib (≤1 μM) low-dose regorafenib exerts unique bioactive effects.[48,49] Based on previous references and our prior experiments, we chose a 0−800 nM of regorafenib concentration for the cellular experiments. As illustrated in Figure 6C,D, compared to the RANKL controls, a marked decrease in TRAcP-stained positive multinucleated cells was observed in both BMMs and RAW 264.7 cells treated with regorafenib. After treatment with regorafenib, a concentration-dependent reduction in the number of TRAcP-stained positive multinucleated cells was observed in both BMMs and RAW 264.7 cells (Figure 6E,F). For BMMs, compared with the RANKL controls, this reduction commenced at a concentration of 100 nM (P = 0.009), with the most substantial decreases observed at 200, 400, and 800 nM (P = 0.001; P = 0.000; P = 0.000). In RAW 264.7 cells, the reduction began at 200 nM (P = 0.009), with the most significant decreases noted at 400 and 800 nM (P = 0.000; P = 0.000). In particular, at a concentration of 800 nM, the number of TRAcP-stained positive multinucleated cells in BMMs and RAW 264.7 cells was reduced by more than 50% compared to the RANKL controls. Additionally, a CCK8 assay was employed to assess cell viability and the potentially toxic effects of regorafenib on BMMs and RAW 264.7 cells. As shown in Figure 6A,B, no toxic effects were exhibited by regorafenib on the BMMs and RAW 264.7 cells at concentrations of 800 nM or below (P > 0.05). These findings provided that regorafenib effectively suppressed RANKL-induced osteoclast formation in vitro, and its toxicity did not mediate this inhibitory effect.

4.5. Regorafenib Attenuated Bone Resorptive Function of Osteoclasts. To examine the impact on osteoclast bone resorption, we investigated whether regorafenib affected the formation of F-actin rings in osteoclasts, a crucial feature for bone resorption during osteoclastogenesis.[50] Following RANKL stimulation, BMM cells differentiated into mature osteoclasts, characterized by larger and morphologically intact F-actin ring structures. However, in the regorafenib treatment groups at concentrations of 400 and 800 nM, we observed a significant decrease in the area of F-actin ring structures compared to the RANKL controls (P = 0.001; P = 0.000; Figure 7A,B).

Next, we examined the effects of regorafenib on the formation of bone resorption pit on the bovine bone slices. Quantitative analysis revealed that RANKL stimulation increased the number of bone resorptive pits. Conversely, treatment with 400 and 800 nM regorafenib significantly reduced the number of bone resorption pits compared to the RANKL controls (P = 0.001; P = 0.000; Figure 8A,B). Overall, our findings demonstrated that regorafenib could effectively hamper bone resorptive activity during osteoclastogenesis.

https://doi.org/10.1021/acsomega.4c01308
ACS Omega 2024, 9, 33574−33593

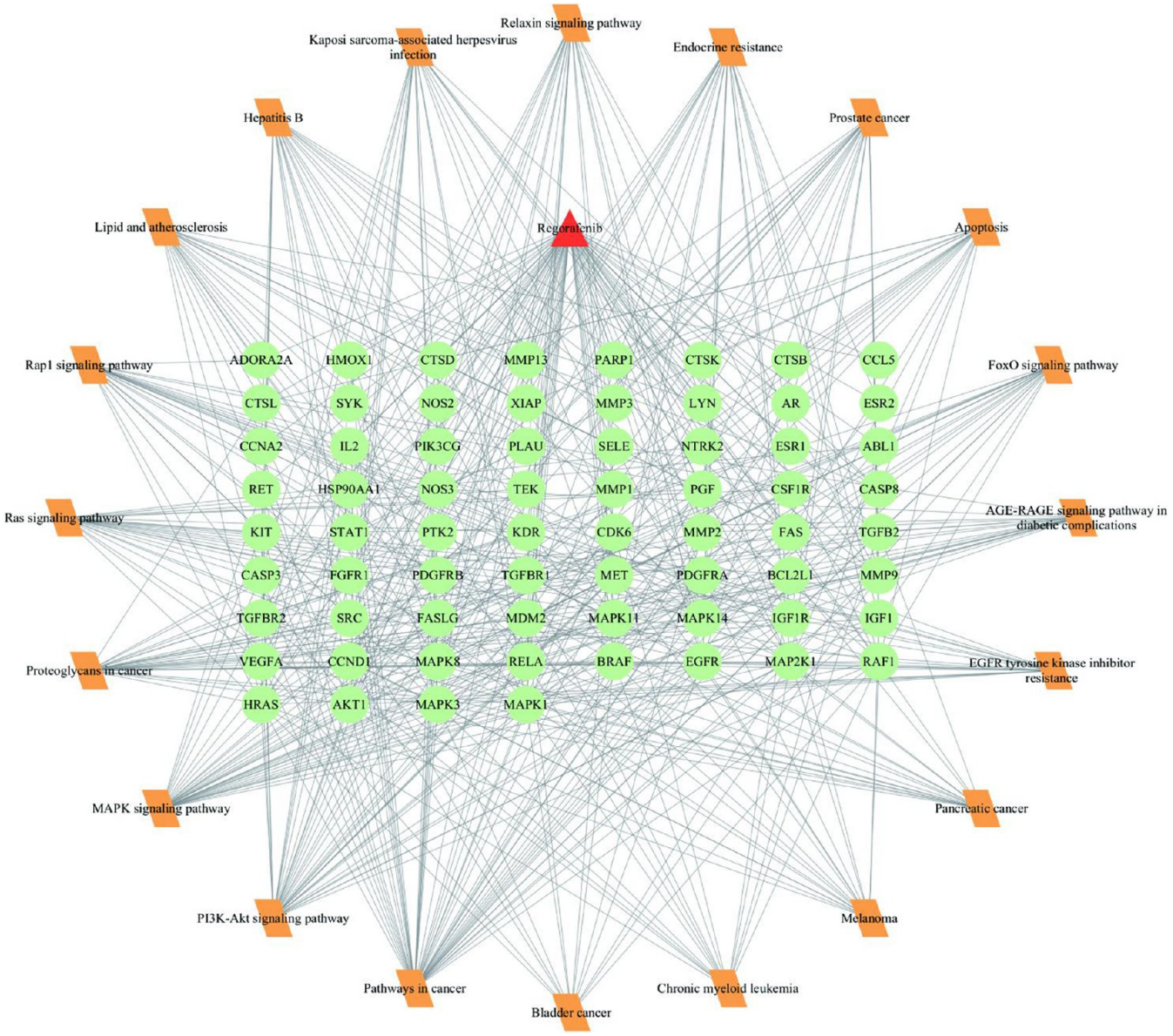

Figure 4. Drug-target-pathway network. The green circles represent target genes, and the orange parallelograms represent pathways.

4.6. Regorafenib Inhibited RANKL-Induced NFAT Signaling Pathway. NFATc1, a member of the NFAT family, plays a pivotal role in the differentiation and maturation of osteoclasts.[51] The results of the NFAT luciferase reporter gene assay demonstrated that compared with both the control and RANKL controls, regorafenib inhibited the transcriptional activity of NFATc1 after treatment with regorafenib ($P < 0.05$) (Figure 9A). Furthermore, as shown in Figure 9C,D, results from the Western blot assay revealed that the level of NFATc1 protein expression was also found to be suppressed after treatment with regorafenib, especially at the concentrations of 800 nM ($P = 0.02$). These results suggested that regorafenib could inhibit NFAT signaling pathways mediated by RANKL, impacting osteoclast maturation and activity.

4.7. Regorafenib Down-Regulated the Level of Osteoclast-Specific Gene Expression. The above experiments revealed that regorafenib could inhibit osteoclast differentiation by suppressing the NFAT signaling pathway. To further investigate the effects of regorafenib on osteoclast-specific genes, we utilized qRT-PCR to detect its impact on the level of NFATc1 and its downstream genes V-ATPase-d2, Cathepsin K and TRAcP with a treatment of 800 nM regorafenib. Notably, RANKL stimulation caused a remarkable increase in the expression of osteoclast-specific genes compared to the control groups. However, regorafenib treatment caused a noteworthy decrease in the expression levels of these genes (Figure 9E−H). Regorafenib exerted inhibitory effects on the expression of NFATc1 ($P = 0.026$), as well as its downstream genes such as V-ATPase-d2 ($P = 0.000$), Cathepsin K ($P = 0.000$), and TRAcP ($P = 0.001$). Conclusively, regorafenib could exhibit inhibition in the activation of NFATc1, thereby impacting the expression of downstream transcriptional genes.

4.8. Regorafenib Inhibited RANKL-Induced MAPK and NF-κB Signaling Pathways. The RANKL/RANK pathway is essential for osteoclast differentiation and involves critical signaling pathways such as NF-κB, ERK, JNK, and p38.[52] To gain deeper insight into the potential molecular mechanism underlying regorafenib's inhibition of RANKL-induced osteoclastogenesis, we employed Western blotting to

https://doi.org/10.1021/acsomega.4c01308
ACS Omega 2024, 9, 33574−33593

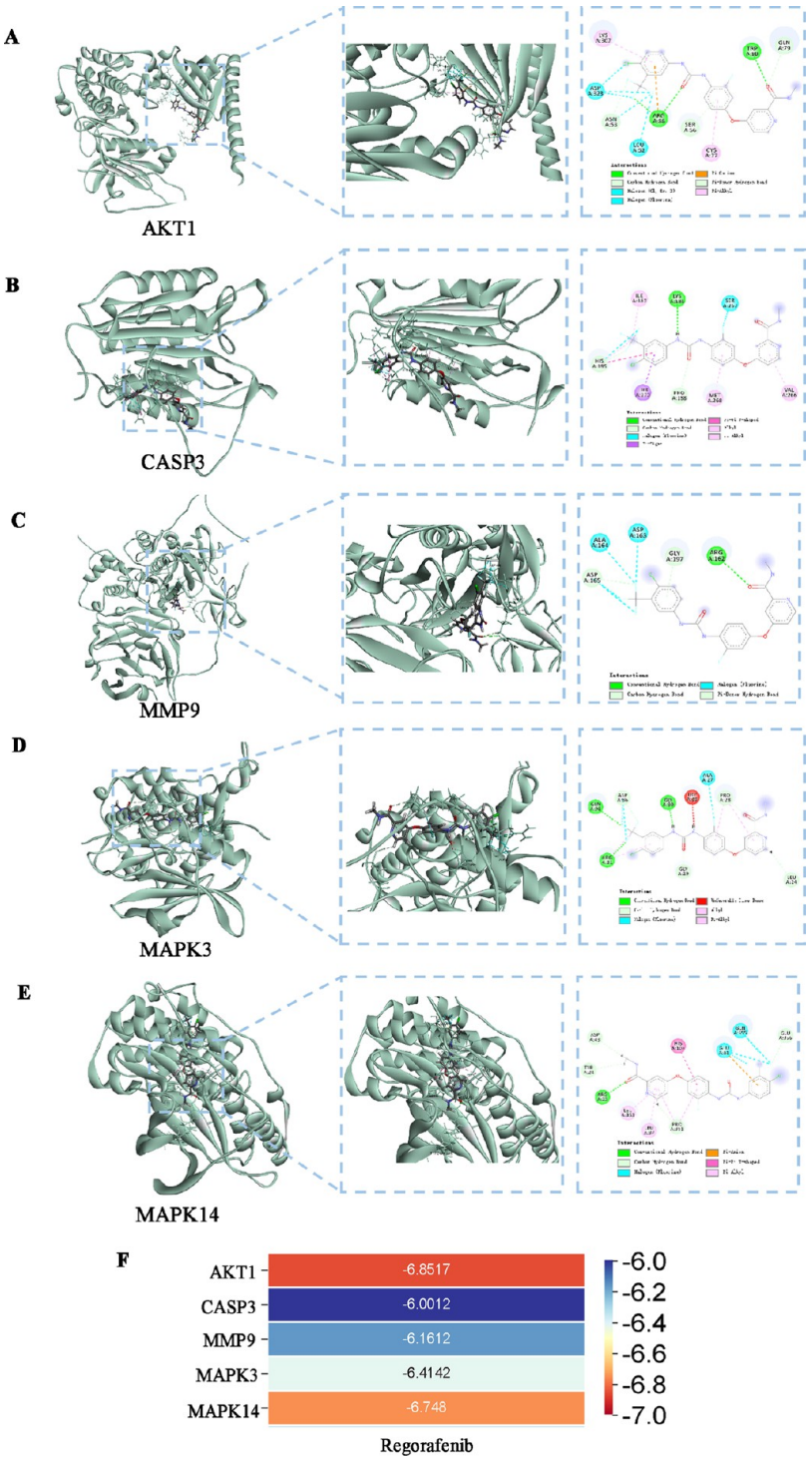

Figure 5. Molecular docking verification of the key targets. (A−E) Mode of AKT1, CASP3, MMP9, MAPK3, MAPK14 interacting with regorafenib. (F) Heatmap of the binding energy score. Red signifies strong binding, and blue represents weaker binding strength. The deeper the shade of red, the stronger the binding capacity.

detect the effect of regorafenib on RANKL-induced NF-κB and MAPK pathways. We observed that treatment with 800 nM regorafenib inhibited the degradation of IκB-α protein, particularly at 5 min of RANKL stimulation (P = 0.045), indicating that regorafenib also exerted inhibitory effects on NF-κB activation (Figure 10A,B). Consistent with this result, the results of luciferase reporter gene assay showed that the transcriptional activity of NF-κB was significantly reduced by regorafenib (P < 0.05, Figure 9B).

As shown in the results (Figure 10C−F), compared with the RANKL group, treatment with 800 nM regorafenib inhibited the phosphorylation of ERK and p38 proteins. The ratio of phosphorylated ERK to total ERK was markedly suppressed by regorafenib at 5 and 10 min of RANKL stimulation (P = 0.049; P = 0.048). The ratio of phosphorylated p38 to total p38 decreased noticeably, with the most significant effects observed at 20, 30, and 60 min after RANKL stimulation (P = 0.002; P = 0.003; P = 0.014). Interestingly, no significant effect was

https://doi.org/10.1021/acsomega.4c01308
ACS Omega 2024, 9, 33574−33593

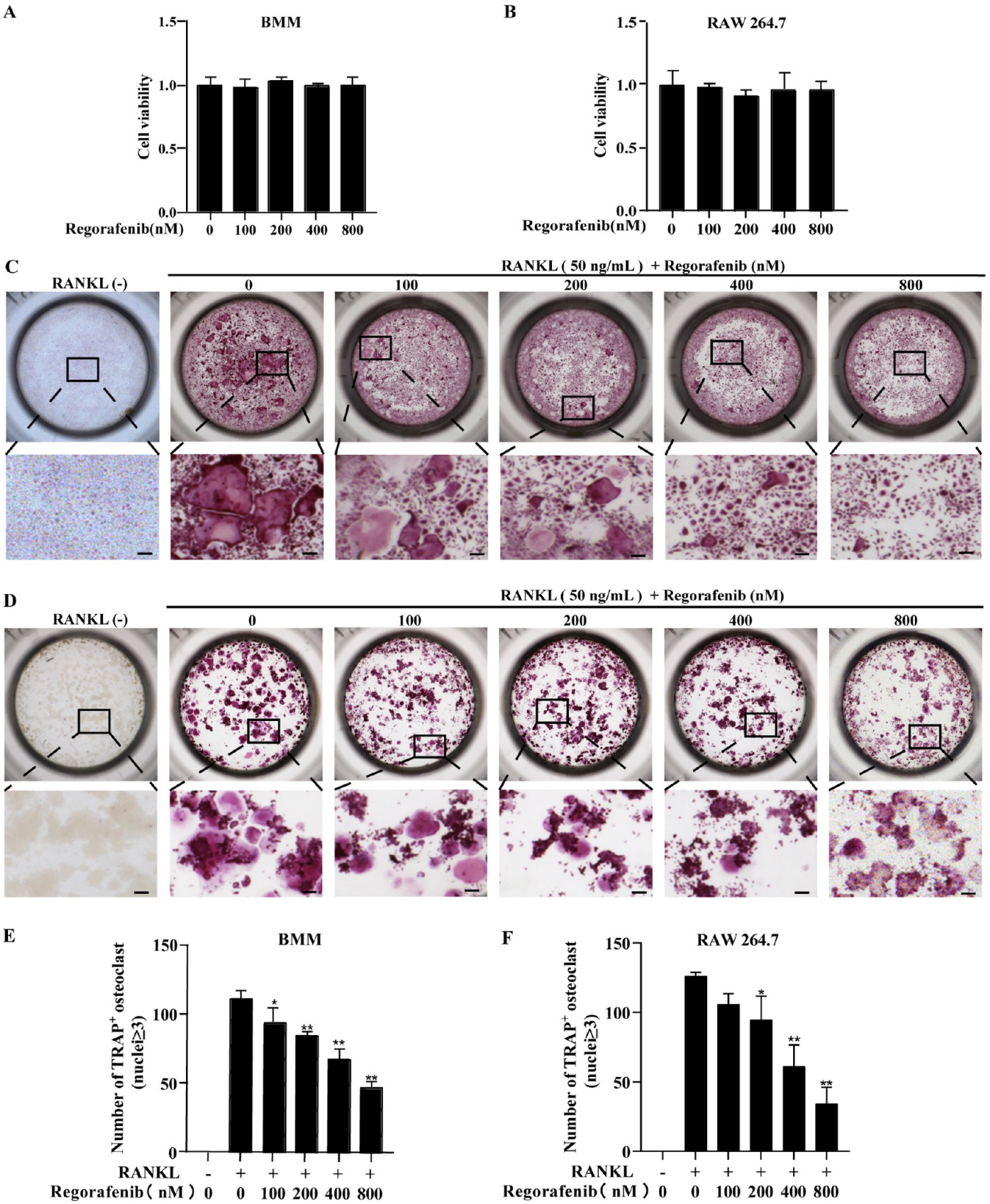

Figure 6. Regorafenib suppressed RANKL-induced osteoclast formation in vitro. (A, B) CCK-8 assay of BMMs and RAW264.7 cells. (C, D) Representative images of TRAcP staining of BMMs and RAW264.7 cell. Scale bar = 200 μm. (E, F) Quantification of BMMs and RAW264.7 cells induced TRAcP positive multinucleated osteoclasts (Nuclei ≥ 3). (Data are presented as mean ± SD (n = 3). Differences among groups were analyzed using a one-way ANOVA test. *P < 0.05, **P < 0.01 relative to the RANKL controls).

observed on the JNK signaling pathways (P > 0.05). These results suggested that regorafenib exerted an inhibitory effect via pERK, p38, and NF-κB signaling pathways mediated by RANKL.

https://doi.org/10.1021/acsomega.4c01308
ACS Omega 2024, 9, 33574−33593

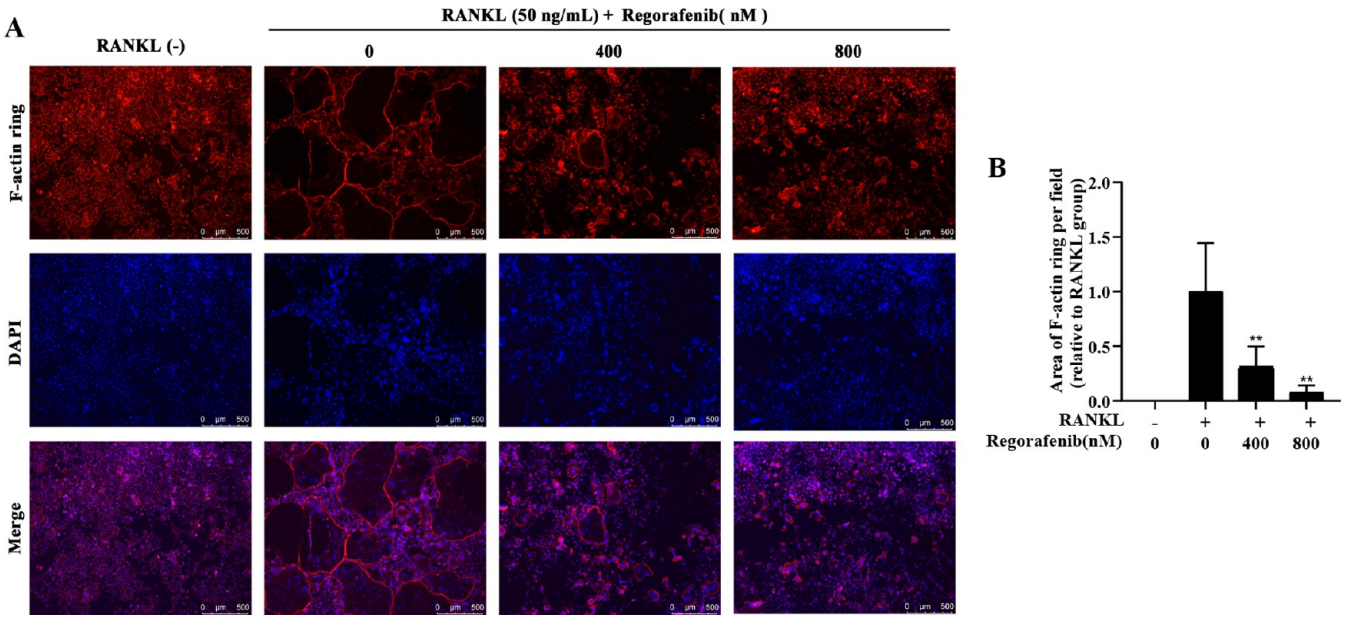

Figure 7. Regorafenib inhibited the formation of the F-actin ring of osteoclasts induced by RANKL. (A) Representative images of phalloidin staining in a fluorescence microscope. Scale bar = 500 μm. (B) Quantification of F-actin ring area per field. (Data are presented as mean ± SD (n = 6). Differences among groups were analyzed using a one-way ANOVA test. *P < 0.05, **P < 0.01 relative to the RANKL controls).

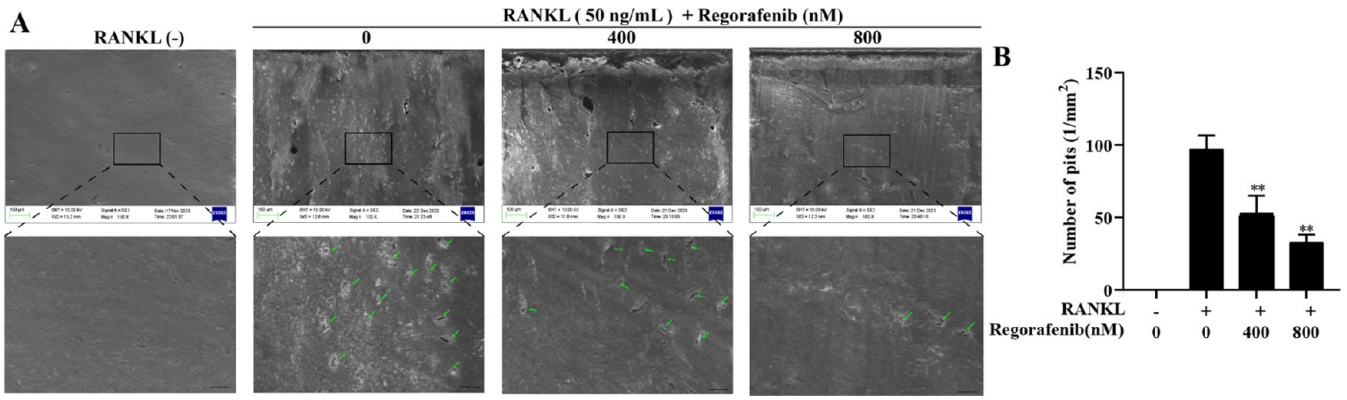

Figure 8. Regorafenib inhibited the bone resorptive function of osteoclasts. (A) Representative images of bone resorption pits. The green arrows represent the bone resorption pits. Scale bar = 100 μm. (B) Quantification of the number of bone resorption pits per well. (Data are presented as mean ± SD (n = 3). Differences among groups were analyzed using a one-way ANOVA test. *P < 0.05, **P < 0.01 relative to the RANKL controls).

4.9. Regorafenib Alleviated Bone Loss in Ovariectomized Mice Model. Our study established an ovariectomized mice model to evaluate the potential therapeutic effect of regorafenib against bone loss. Throughout the initial modeling and the 6-week treatment period, no adverse events or fatalities were observed in each group. Micro-CT results revealed that, compared to the sham operation group, mice in the OVX group exhibited an expansion of the femoral trabecular gap and a reduction in bone volume (Figure 11A), indicating the successful establishment of the ovariectomy-induced bone loss mice model. Compared to the OVX group, the OVX mice treated with regorafenib showed improvements in femoral trabecular gap width and increased bone mass. Quantitative analysis confirmed that compared with the OVX group, measures including BV/TV, BS/TV, and Tb.N all showed improvements (Figure 11B–D). Conversely, Tb.Sp decreased (Figure 11E). H&E staining examination suggested that regorafenib treatment significantly mitigated the bone loss induced by ovariectomy compared to the OVX group (Figure 12A). BV/TV in the OVX group was significantly lower than in the sham-operated group, whereas treatment with regorafenib substantially elevated BV/TV, as shown in Figure 12B (P = 0.011). Besides, the results of TRAcP staining showed that after treatment with regorafenib, the surface area of osteoclasts per unit of bone surface (Oc.s/Bs) was reduced as opposed to the OVX group (P = 0.000) (Figure 12C,D). These results demonstrated that regorafenib may have a protective effect against bone mass loss by inhibiting osteoclast activity in vivo.

5. DISCUSSION

Postmenopausal osteoporosis is one of the most common osteoclast-related osteolytic diseases that manifests with bone loss and pathological fractures. Prior research indicated that approximately half of postmenopausal females afflicted by osteoporosis, and the rate of fracture due to the disease reaches up to 40%.[5] The high prevalence and serious complications of this condition underscore the urgent necessity for innovative

https://doi.org/10.1021/acsomega.4c01308
ACS Omega 2024, 9, 33574−33593

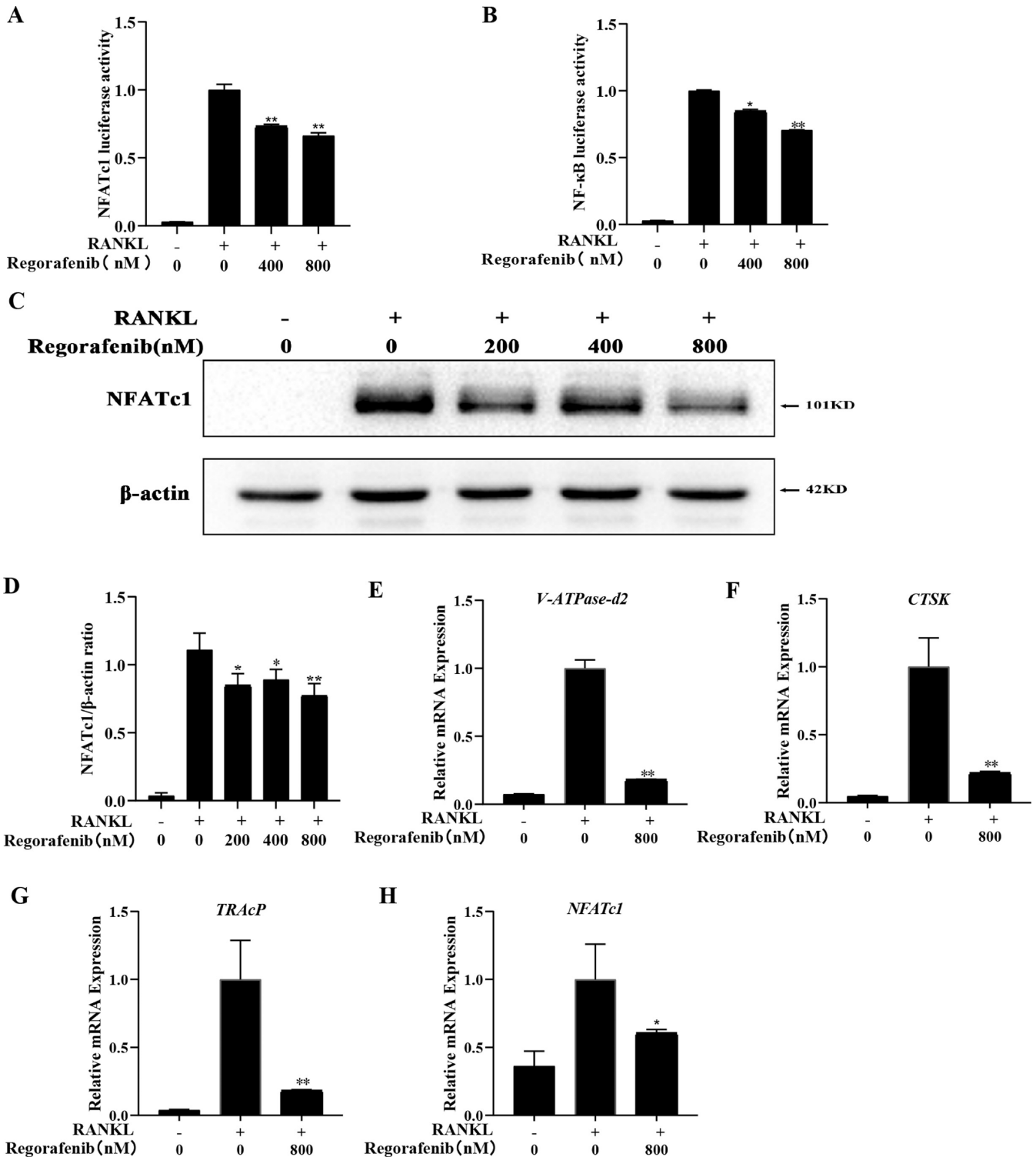

Figure 9. Regorafenib inhibited RANKL-induced NFAT signaling pathway and the expression of osteoclast-specific genes. (A) Quantitative analysis of the luciferase activities of NFATc1. (B) Quantitative analysis of the luciferase activities of NF-κB. (C) Representative images of NFATc1 protein expression. (D) Quantitative analysis of NFATc1 expression normalized to β-actin. (E–H) Statistical results of osteoclast-specific gene expression, including V-ATPase-d2, CTSK, TRAcP, and NFATc1. (Data are presented as mean ± SD (n = 3). Differences among groups were analyzed using a one-way ANOVA test. *P < 0.05, **P < 0.01 relative to the RANKL controls).

therapeutic strategies aimed at managing osteoclast-related osteolytic diseases.

Regorafenib, as a multitargeted tyrosine kinase inhibitor, is gradually being discovered to have potential curative effects in animal models of pulmonary emphysema,[53] pulmonary hypertension,[54] autoimmune arthritis,[55] and Alzheimer's disease.[56] Given its established antitumor properties, exploring regorafenib's utility in noncancerous diseases is of significant scientific interest. However, its role in osteoclast-related osteolytic diseases is unclear. The current study first reveals

https://doi.org/10.1021/acsomega.4c01308
ACS Omega 2024, 9, 33574−33593

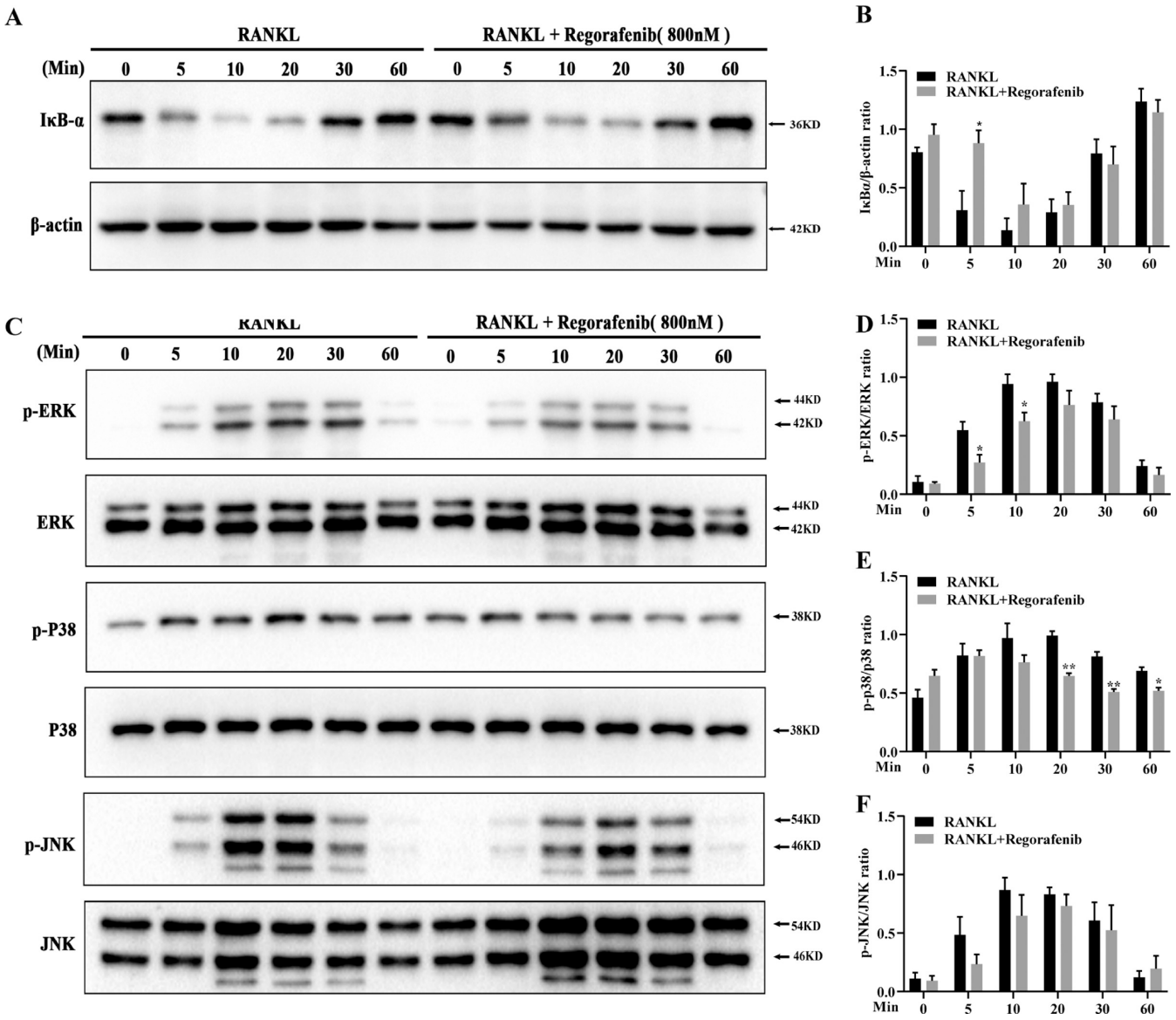

Figure 10. Regorafenib inhibited RANKL-induced osteoclastogenesis by suppressing NF-κB and MAPK signaling pathways. (A) Representative images of IκB-α protein expression. (B) Quantitative analysis of IκB-α expression normalized to β-actin. (C) Representative pictures of p-ERK and ERK, p-P38 and p38, and p-JNK and JNK protein expression. (D−F) Statistical results of the ratios of phosphorylated ERK, p38, and JNK relative to their respective total proteins. (Data are presented as mean ± SD (n = 3). Statistical analyses between the RANKL controls and the regorafenib-treatment group were analyzed by a two-tailed Student's t test. *P < 0.05, **P < 0.01 relative to the RANKL controls).

that regorafenib exhibits therapeutic potential for osteoclast-related osteolytic disease by inhibiting osteoclastogenesis through the suppression of NF-κB, NFAT, ERK, and p38 signaling pathways.

Extensive research has validated the inhibitory impact of numerous multitargeted tyrosine kinase inhibitors on bone resorption and loss, suggesting potential therapeutic advantages for bone disease management. For example, dasatinib has been shown to forestall joint destruction in models of rheumatoid arthritis by impeding osteoclastogenesis,[57] while also enhancing bone volume in xenograft mice models infused with osteotropic MDA-MB-231 cells by diminishing osteoclast activity.[58] Similarly, the tyrosine kinase inhibitor GNF-2 was observed to inhibit osteoclast differentiation by curtailing RANKL-induced NF-κB signaling, thereby offering protection against inflammation-induced bone destruction.[59] Distinguished from prior investigations, considering the complexity of regorafenib targets, this study uniquely integrates network pharmacology and experimental methodologies to scrutinize the effects and underlying mechanisms of regorafenib on osteoclast-related osteolytic diseases.

Network pharmacology, an emerging discipline that merges knowledge from fields such as bioinformatics, systems biology, and various omics, furnishes novel perspectives for elucidating drug-disease interaction mechanisms.[60,61] In our study, a total of 89 common intersect targets as potential regorafenib therapeutic targets against osteoclast-related osteolytic diseases were obtained by network pharmacology. Subsequent PPI analysis, GO functional annotation, and KEGG pathway enrichment analysis shed light on regorafenib's mechanism in acting on osteoclast-related osteolytic diseases. This mechanism likely involves the modulation of pivotal targets such as AKT1, CASP3, MMP9, ESR1, and MAPK3, and the regulation of biological processes including protein activity, phosphor-

https://doi.org/10.1021/acsomega.4c01308
ACS Omega 2024, 9, 33574−33593

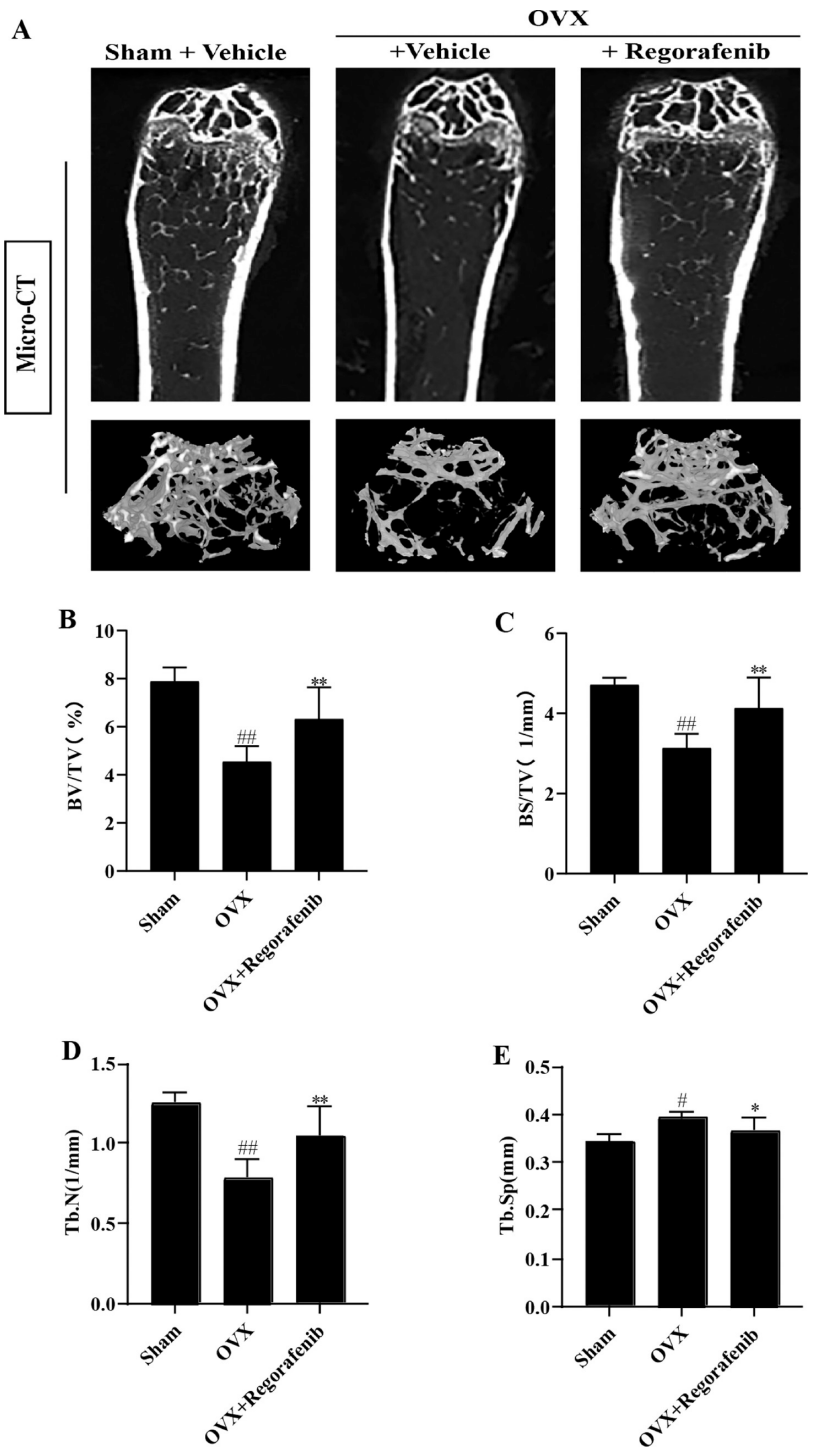

Figure 11. Regorafenib had a protective effect against bone loss in vivo. (A) Representative pictures of Micro-CT on mouse femurs in sham, OVX, and OVX + regorafenib group. (B−E) Statistical analysis of the parameters with bone structural, including BV/TV, BS/TV, TB.N, and Tb.Sp. (Data are presented as mean ± SD (n = 6). Differences among groups were analyzed using a one-way ANOVA test. *P < 0.05, **P < 0.01, #P < 0.05, ##P < 0.01, *relative to the OVX groups, #relative to the sham groups).

ylation, and apoptosis, alongside influencing key signaling pathways such as cancer, MAPK, PI3K-Akt, apoptosis, TNF signaling, and osteoclast differentiation. Notably, the MAPK, PI3K-Akt, apoptosis, and osteoclast differentiation pathways have been identified as crucial regulators of osteoclastogenesis.[62−64]

To further validate the above results, we performed cellular and animal experiments. Through cellular experiments, we found for the first time that regorafenib imposed its inhibitory effect on osteoclast differentiation and its bone resorption function without no toxic effects on both BMMs and RAW 264.7 cells. These findings imply that regorafenib could be a promising and relatively safe therapeutic approach for osteolytic diseases.

Considering the critical role of the RANKL/RANK signaling pathway in osteoclast formation, we performed a series of

https://doi.org/10.1021/acsomega.4c01308
ACS Omega 2024, 9, 33574−33593

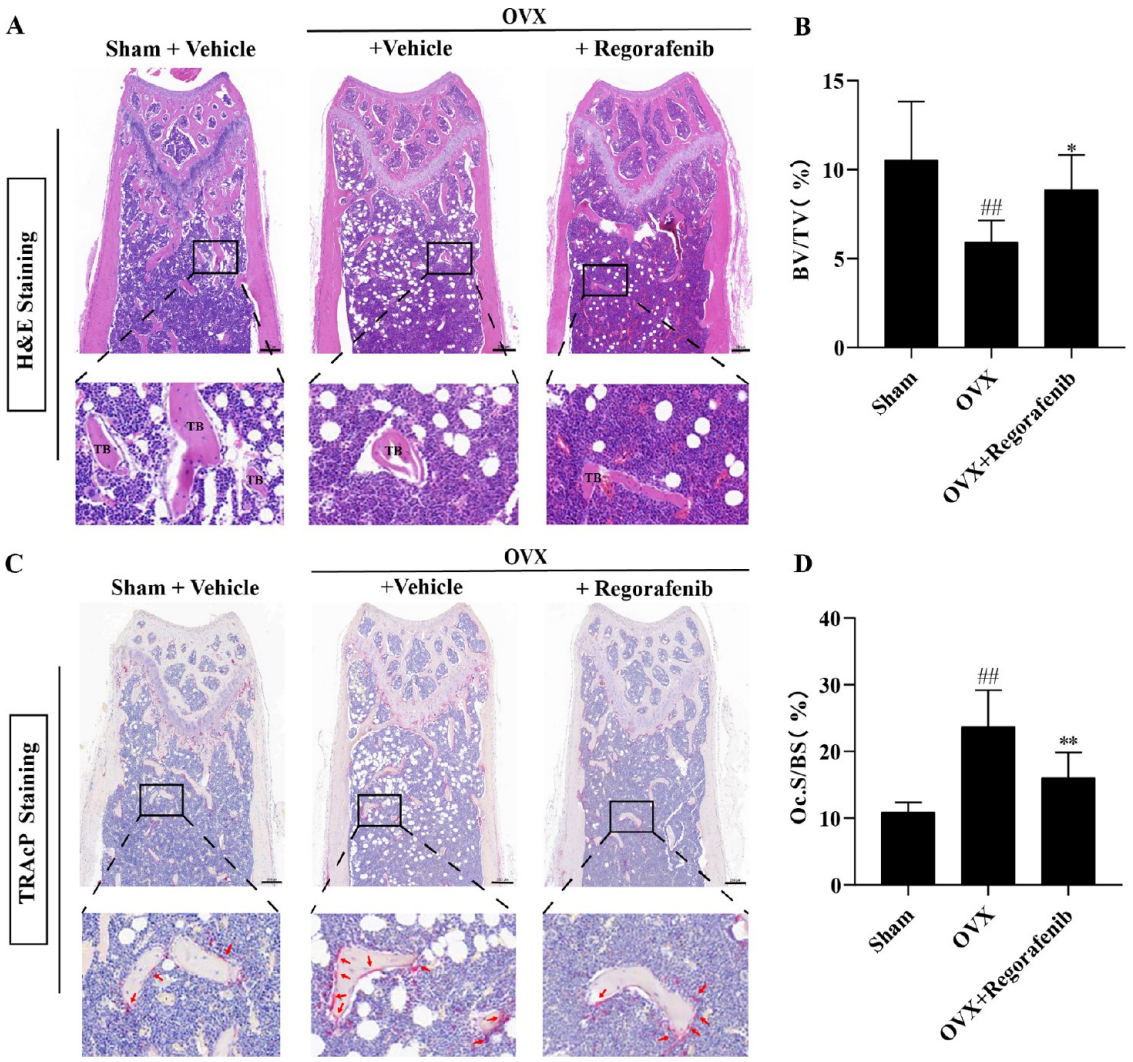

Figure 12. Regorafenib alleviated the ovariectomy-induced bone loss by inhibiting the activity of osteoclasts. (A) Representative pictures of H&E staining for femoral sections each group. TB represented the bone trabecular. Scale bar = 200 μm. (B) Quantitative results of BV/TV with H&E staining. (C) Representative images of femur sections stained with TRcAP of each group. The red arrows indicate TRAcP-positive osteoclasts. Scale bar = 200 μm. (D) Quantitative results of the area of TRAcP-positive cells per trabecular surface (Oc.S/BS). (Data are presented as mean ± SD (n = 6). Differences among groups were analyzed using a one-way ANOVA test. *P < 0.05, **P < 0.01, #P < 0.05, ##P < 0.01, *relative to the OVX groups, #relative to the sham groups).

molecular biology experiments. By integrating the result of network pharmacology analysis, it was deduced that the majority of these key targets are connected with the MAPK signaling pathway, insinuating that the MAPK signaling may be intimately associated with the onset and progression of osteoclast-related osteolytic disease when treated with regorafenib. The MAPK pathway, renowned for its regulatory influence on cellular proliferation and differentiation, also plays an integral role in osteoclast development.[65] The engagement of RANKL with RANK catalyzes the phosphorylation of MAPKs, incorporating proteins such as JNK, p38, and ERK.[66] Numerous studies have corroborated that the inhibition of p38, JNK, or ERK can significantly curtail osteoclast formation.[67−69] Additionally, regorafenib has been identified to impede tumor progression by inhibiting the p38 and ERK signaling pathways. Our investigation demonstrated that regorafenib substantially suppressed the activation of phosphorylated p38 and ERK in RANKL-induced osteoclastogenesis. Furthermore, the molecular docking assay provided evidence that regorafenib could bind with MAPK signaling factors such as MAPK3 and MAPK14 by forming various chemical bonds. Notably, MAPK3/MAPK1, also known as ERK1/ERK2, is a classic and extensively studied signaling pathway within the MAPK signaling pathway.[67] P38α, identified as MAPK14, exhibits high expression levels in osteoclasts.[70] These results suggested that regorafenib exerted its inhibitory impact on osteoclast differentiation through the suppression of the MAPK signaling pathway.

Additionally, the binding of RANKL and RANK activates the NF-κB signaling pathway and promotes the differentiation and maturation of osteoclasts, suggesting that NF-κB is a critical mediator in enhancing osteoclast activity. Moreover, NFATc1 is a key downstream effector of the RANK/RANKL signaling pathway. Activation of the NF-κB and MAPK pathways can promote NFATc1 activation, which enhances transcription factor expression and plays a critical role in the physiological processes of osteoclast differentiation, maturation, and resorption. Our study found that regorafenib could inhibit the degradation of IκB-α protein and decrease the transcriptional activity of NF-κB. Besides, regorafenib could

https://doi.org/10.1021/acsomega.4c01308
ACS Omega 2024, 9, 33574−33593

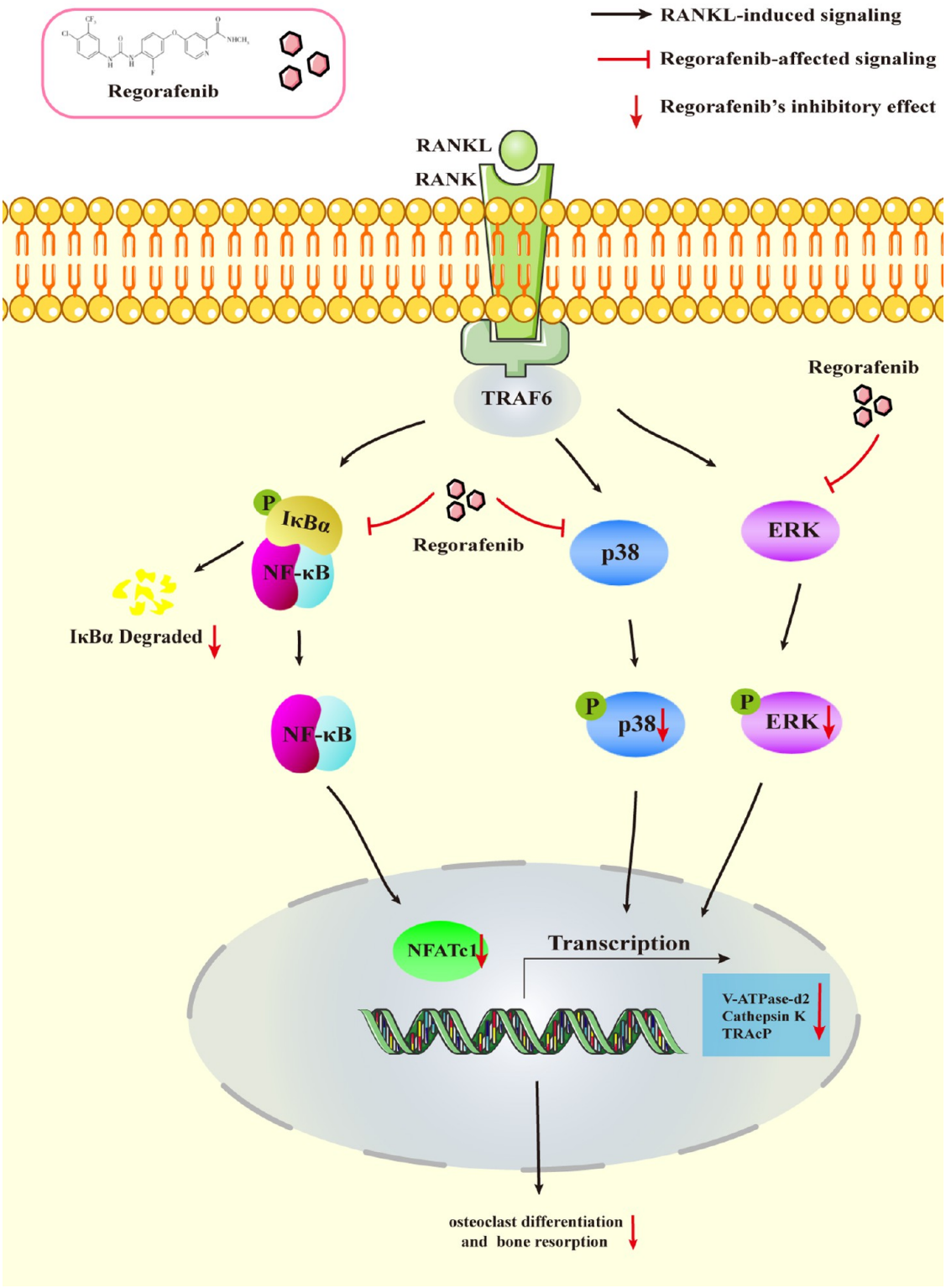

Figure 13. Mechanism diagram of regorafenib modulates RANKL-induced osteoclast differentiation via the NF-κB, NFAT, ERK, and p38 signaling pathways. RANK, receptor activator of nuclear factor-κB; RANKL, RANK ligand; NF-κB, nuclear factor-κB; Iκ B-α, inhibitor of κB-α; NFATc1, nuclear factor of activated T cells 1; p38, p38 kinase; ERK, extracellular regulated protein kinases; V-ATPase d2, Vacuolar ATPase d2; TRAcP, tartrate-resistant acid phosphatase.

downregulate the level of NFATc1 expression as well as its downstream osteoclast-specific genes V-ATPase-d2, Cathepsin K, and TRAcP. These findings indicate that regorafenib exerts its inhibitory effect on osteoclastogenesis by inhibiting the RANKL-induced NF-κB and NFAT signaling pathways and hindering the transcriptional regulation of osteoclast-specific genes by NFATc1 transcription factors.

The ovariectomized mouse model, a classical model for osteoporosis, primarily mimics the environment of decreased osteoclasts and bone loss in estrogen-deficient states.[71] To

https://doi.org/10.1021/acsomega.4c01308
ACS Omega 2024, 9, 33574−33593

further investigate the effects of regorafenib on bone loss in vivo, an ovariectomized mouse model of osteoporosis was established, and regorafenib was administered from the beginning to examine its effect on osteoclastogenesis and bone loss. Both micro-CT results and H&E histochemical staining showed that the treatment with regorafenib could protect against bone loss, elevate the bone volume fraction and the number of trabeculae, reduce trabecular separation and diminish the destruction of bone microstructure. TRAcP staining results suggested that regorafenib significantly reduced the number of osteoclasts, which was consistent with the results in vitro. These suggest that treatment with regorafenib may mitigate ovariectomy induced bone loss in mice by inhibiting osteoclast activity.

Bone homeostasis is a complex process encompassing osteoblastic bone formation and osteoclastic bone resorption.[72] Regorafenib, a multitargeted tyrosine kinase inhibitor, while synthetic, shares similar biological targets with certain natural products.[73,74] It has been shown to target several kinases involved in tumor growth and metastasis, such as VEGFR and CSF1R,[20,26] which are also critical in bone metabolism pathways. This regulation potentially affects osteoclastogenesis and osteoblast activity, suggesting a possible dual role in promoting bone formation and reducing bone resorption. Our study demonstrates that regorafenib can prevent bone loss in ovariectomized mice by inhibiting the activity of osteoclasts, suggesting its potential anticatabolic effects. In addition, some multitargeted tyrosine kinase inhibitors have been found to regulate osteoblasts, thereby influencing bone homeostasis. For example, Antonio Garcia-Gomez found that low-dose dasatinib could promote osteoblast differentiation and its function.[75] Conversely, Kroschwald LM found that imatinib mesylate and nilotinib impair bone metabolism by attenuating osteoblast function in vitro.[76] It is evident that the regulation of osteoblasts by multitargeted tyrosine kinase varies depending on their drug properties and concentrations. Therefore, exploring how regorafenib regulates osteoblasts and bone metabolism and investigating whether it has pro-anabolic effects will be the key focus of our future research.

There are some limitations in our current study. First, future research is needed to explore the underlying mechanisms of signaling cross-talk with additional targets, such as AKT and PI3K, to enrich our understanding of precise targets that regulate these signals. Additionally, future studies should investigate the effects of regorafenib on various osteolytic models, such as bone metastasis models and inflammatory bone disease models, to broaden our understanding of its impact on different osteolytic diseases.

6. CONCLUSIONS

In the current study, we integrated network pharmacology, molecular docking, cellular and animal experiments to predict and validate the targets and mechanisms of regorafenib in treating osteoclast-related osteolytic diseases. The results of network pharmacology reveal that regorafenib may act on osteoclast-related osteolytic diseases through MAPK, PI3K-Akt, apoptosis, TNF signaling, and osteoclast differentiation signaling pathways. And regorafenib showed strong binding affinities to key targets involved in osteoclast activity, such as MAPK3 and MAPK14. Through experimental study, our research demonstrates that regorafenib could inhibit osteoclast differentiation and bone resorption ($P < 0.05$) in dose-dependently without no toxic effects on RAW 264.7 and BMMs. These effects might be achieved via inhibiting RANKL-induced NF-κB, NFAT, ERK, and p38 signaling pathways (Figure 13). The efficacy of regorafenib was corroborated in an ovariectomized mouse model where regorafenib treatment significantly improved bone microarchitecture and bone loss. Notably, regorafenib significantly improved BV/TV, BS/TV, and TB.N, as well as reduced Tb.Sp compared to the OVX groups ($P < 0.05$). Our study evaluates the potential of regorafenib in modulating bone remodeling processes, mainly by inhibiting the pathways that promote osteoclast differentiation and activity. Our research offers promising evidence supporting the development and clinical application of regorafenib in treating osteoclast-related osteolytic diseases, such as osteoporosis and bone metastasis. Moreover, it offers new theoretical bases and innovative ideas for the application of regorafenib development in nononcology fields, highlighting its potential beyond cancer treatment. This study not only contributes to the understanding of regorafenib's mechanism of action in bone disease but also opens avenues for further research and development in the field of bone disease treatment.

■ ASSOCIATED CONTENT

Data Availability Statement

The data sets presented in this study can be found in online repositories. The data sets generated during and/or analyzed during the current study are available from the First author and corresponding author upon reasonable request.

Supporting Information

The Supporting Information is available free of charge at https://pubs.acs.org/doi/10.1021/acsomega.4c01308.

Abbreviations comparison table; the targets of regorafenib (Table S1); the targets of osteolytic diseases (Table S2); the targets of osteoclast (Table S3); intersecting targets of regorafenib and osteoclast-related osteolytic diseases (Table S4); parameters of key targets in PPI (Table S5); information on GO enrichment analysis (Table S6); information on KEGG enrichment analysis (Table S7); and graphical abstract (Figure S1) (PDF)

■ AUTHOR INFORMATION

Corresponding Authors

Chunping Zeng − *Department of Endocrinology, Key Laboratory of Biological Targeting Diagnosis, Therapy and Rehabilitation of Guangdong Higher Education Institutes, The Fifth Affiliated Hospital of Guangzhou Medical University, Guangzhou 510700 Guangdong, China*; Email: zcp193@163.com

Ge Li − *Department of Endocrinology, The Affiliated Shunde Hospital of Jinan University, Foshan 528305 Guangdong, China*; orcid.org/0009-0009-2567-6756; Email: ligeyisheng2019@163.com

Authors

Lin Zhou − *Department of Endocrinology, Key Laboratory of Biological Targeting Diagnosis, Therapy and Rehabilitation of Guangdong Higher Education Institutes, The Fifth Affiliated Hospital of Guangzhou Medical University, Guangzhou 510700 Guangdong, China*

https://doi.org/10.1021/acsomega.4c01308
ACS Omega 2024, 9, 33574−33593

Peiru Su − *Department of Endocrinology, Key Laboratory of Biological Targeting Diagnosis, Therapy and Rehabilitation of Guangdong Higher Education Institutes, The Fifth Affiliated Hospital of Guangzhou Medical University, Guangzhou 510700 Guangdong, China*

Xiangya Luo − *Department of Endocrinology, Key Laboratory of Biological Targeting Diagnosis, Therapy and Rehabilitation of Guangdong Higher Education Institutes, The Fifth Affiliated Hospital of Guangzhou Medical University, Guangzhou 510700 Guangdong, China*

Xuanli Zhong − *Department of Endocrinology, The Affiliated Shunde Hospital of Jinan University, Foshan 528305 Guangdong, China*

Qian Liu − *Guangxi Key Laboratory of Regenerative Medicine, Guangxi Medical University, Nanning 530021 Guangxi, China*

Yuangang Su − *Guangxi Key Laboratory of Regenerative Medicine, Guangxi Medical University, Nanning 530021 Guangxi, China*

Complete contact information is available at: https://pubs.acs.org/10.1021/acsomega.4c01308

Author Contributions

[‖]L.Z. and P.S. contributed equally to this work. L.Z.: Data curation, investigation and writing review, editing, and funding acquisition. P.S.: Data curation, investigation, methodology, validation, writing original draft, and editing; X.L.: Formal analysis and investigation. X.Z.: Investigation and supervision. Q.L. and Y.S.: Methodology. C.Z.: Conceptualization and project administration. G.L.: Conceptualization, funding acquisition, and supervision. All authors have read and approved the final manuscript. All authors agree to be accountable for all aspects of the work and ensure its integrity and accuracy.

Funding

This work was supported by Guangdong Basic and Applied Basic Research Foundation (2019A1515110723), Medical Joint Fund of Jinan University (MF220206), and Key Laboratory of Guangdong Higher Education Institutes (2021KSYS009).

Notes

The authors declare no competing financial interest.

■ ACKNOWLEDGMENTS

We are grateful to the Guangxi Key Laboratory of Regenerative Medicine, Guangxi Medical University, for providing guidance and assistance to our research.

■ REFERENCES

(1) Marahleh, A.; Kitaura, H.; Ohori, F.; Noguchi, T.; Mizoguchi, I. The osteocyte and its osteoclastogenic potential. *Front. Endocrinol.* **2023**, *14*, No. 1121727.

(2) Kim, J. M.; Lin, C.; Stavre, Z.; Greenblatt, M. B.; Shim, J. H. Osteoblast-Osteoclast Communication and Bone Homeostasis. *Cells* **2020**, *9* (9), 2073.

(3) Da, W.; Tao, L.; Zhu, Y. The Role of Osteoclast Energy Metabolism in the Occurrence and Development of Osteoporosis. *Front. Endocrinol.* **2021**, *12*, No. 675385.

(4) Győri, D. S.; Mócsai, A. Osteoclast Signal Transduction During Bone Metastasis Formation. *Front. Cell Dev. Biol.* **2020**, *8*, 507.

(5) Li, J.; Chen, X.; Lu, L.; Yu, X. The relationship between bone marrow adipose tissue and bone metabolism in postmenopausal osteoporosis. *Cytokine Growth Factor Rev.* **2020**, *52*, 88−98.

(6) Clézardin, P.; Coleman, R.; Puppo, M.; Ottewell, P.; Bonnelye, E.; Paycha, F.; Confavreux, C. B.; Holen, I. Bone metastasis: mechanisms, therapies, and biomarkers. *Physiol. Rev.* **2021**, *101* (3), 797−855.

(7) Sing, C. W.; Lin, T. C.; Bartholomew, S.; Bell, J. S.; Bennett, C.; Beyene, K.; Bosco-Levy, P.; Bradbury, B. D.; Chan, A. H. Y.; Chandran, M.; et al. Global Epidemiology of Hip Fractures: Secular Trends in Incidence Rate, Post-Fracture Treatment, and All-Cause Mortality. *J. Bone Miner. Res.: Off. J. Am. Soc. Bone Miner. Res.* **2023**, *38* (8), 1064−1075.

(8) Cui, L.; Jackson, M.; Wessler, Z.; Gitlin, M.; Xia, W. Estimating the future clinical and economic benefits of improving osteoporosis diagnosis and treatment among women in China: a simulation projection model from 2020 to 2040. *Arch. Osteoporosis* **2021**, *16* (1), 118.

(9) Munoz, M.; Robinson, K.; Shibli-Rahhal, A. Bone Health and Osteoporosis Prevention and Treatment. *Clin. Obstet. Gynecol.* **2020**, *63* (4), 770−787.

(10) Wang, B.; Zhan, Y.; Yan, L.; Hao, D. How zoledronic acid improves osteoporosis by acting on osteoclasts. *Front. Pharmacol.* **2022**, *13*, No. 961941.

(11) Reid, I. R.; Billington, E. O. Drug therapy for osteoporosis in older adults. *Lancet* **2022**, *399* (10329), 1080−1092.

(12) Ferrari, S.; Langdahl, B. Mechanisms underlying the long-term and withdrawal effects of denosumab therapy on bone. *Nat. Rev. Rheumatol.* **2023**, *19* (5), 307−317.

(13) Xie, G.; Liu, W.; Lian, Z.; Xie, D.; Yuan, G.; Ye, J.; Lin, Z.; Wang, W.; Zeng, J.; Shen, H.; et al. Spleen tyrosine kinase (SYK) inhibitor PRT062607 protects against ovariectomy-induced bone loss and breast cancer-induced bone destruction. *Biochem. Pharmacol.* **2021**, *188*, No. 114579.

(14) Yang, T.; Chen, W.; Gan, K.; Wang, C.; Xie, X.; Su, Y.; Lian, H.; Xu, J.; Zhao, J.; Liu, Q. Myrislignan targets extracellular signal-regulated kinase (ERK) and modulates mitochondrial function to dampen osteoclastogenesis and ovariectomy-induced osteoporosis. *J. Transl. Med.* **2023**, *21* (1), 839.

(15) De Leon-Oliva, D.; Barrena-Blázquez, S.; Jiménez-Álvarez, L.; Fraile-Martinez, O.; García-Montero, C.; López-González, L.; Torres-Carranza, D.; García-Puente, L. M.; Carranza, S. T.; Álvarez-Mon, M.; et al. The RANK-RANKL-OPG System: A Multifaceted Regulator of Homeostasis, Immunity, and Cancer. *Medicina* **2023**, *59* (10), 1752.

(16) McDonald, M. M.; Kim, A. S.; Mulholland, B. S.; Rauner, M. New Insights Into Osteoclast Biology. *JBMR Plus* **2021**, *5* (9), No. e10539.

(17) Veis, D. J.; O'Brien, C. A. Osteoclasts, Master Sculptors of Bone. *Annu. Rev. Pathol.: Mech. Dis.* **2023**, *18* (1), 257−281.

(18) Zhou, W.; Zhou, W.; Bi, Y.; Zhou, Z.; Zhou, Z.; Chen, S.; Xie, G.; Lian, Z.; Yuan, G.; Yao, G. Antidepressant duloxetine hydrochloride protects against ovariectomy-induced bone loss in mice by inhibiting osteoclast differentiation. *Biomed. Pharmacother.* **2023**, *168*, No. 115810.

(19) Ihn, H. J.; Lim, J.; Kim, K.; Nam, S. H.; Lim, S.; Lee, S. J.; Bae, J. S.; Kim, T. H.; Kim, J. E.; Baek, M. C.; et al. Protective Effect of Ciclopirox against Ovariectomy-Induced Bone Loss in Mice by Suppressing Osteoclast Formation and Function. *Int. J. Mol. Sci.* **2021**, *22* (15), 8299.

(20) Grothey, A.; Blay, J. Y.; Pavlakis, N.; Yoshino, T.; Bruix, J. Evolving role of regorafenib for the treatment of advanced cancers. *Cancer Treat. Rev.* **2020**, *86*, No. 101993.

(21) Jiang, J.; Zhang, L.; Chen, H.; Lei, Y.; Zhang, T.; Wang, Y.; Jin, P.; Lan, J.; Zhou, L.; Huang, Z.; et al. Regorafenib induces lethal autophagy arrest by stabilizing PSAT1 in glioblastoma. *Autophagy* **2020**, *16* (1), 106−122.

(22) Weng, M. C.; Wang, M. H.; Tsai, J. J.; Kuo, Y. C.; Liu, Y. C.; Hsu, F. T.; Wang, H. E. Regorafenib inhibits tumor progression through suppression of ERK/NF-κB activation in hepatocellular carcinoma bearing mice. *Biosci. Rep.* **2018**, *38* (3), BSR20171264.

(23) Breitkreutz, I.; Podar, K.; Figueroa-Vazquez, V.; Wilhelm, S.; Hayden, P. J.; Anderson, K. C.; Raab, M. S. The orally available

multikinase inhibitor regorafenib (BAY 73−4506) in multiple myeloma. *Ann. Hematol.* **2018**, *97* (5), 839−849.
(24) Mantovani, A.; Marchesi, F.; Malesci, A.; Laghi, L.; Allavena, P. Tumour-associated macrophages as treatment targets in oncology. *Nat. Rev. Clin. Oncol.* **2017**, *14* (7), 399−416.
(25) Doleschel, D.; Hoff, S.; Koletnik, S.; Rix, A.; Zopf, D.; Kiessling, F.; Lederle, W. Regorafenib enhances anti-PD1 immunotherapy efficacy in murine colorectal cancers and their combination prevents tumor regrowth. *J. Exp. Clin. Cancer Res.* **2021**, *40* (1), 288.
(26) Wen, J.; Wang, S.; Guo, R.; Liu, D. CSF1R inhibitors are emerging immunotherapeutic drugs for cancer treatment. *Eur. J. Med. Chem.* **2023**, *245* (Pt 1), No. 114884.
(27) Hume, D. A.; Batoon, L.; Sehgal, A.; Keshvari, S.; Irvine, K. M. CSF1R as a Therapeutic Target in Bone Diseases: Obvious but Not so Simple. *Curr. Osteoporos Rep.* **2022**, *20* (6), 516−531.
(28) Mun, S. H.; Park, P. S. U.; Park-Min, K. H. The M-CSF receptor in osteoclasts and beyond. *Exp. Mol. Med.* **2020**, *52* (8), 1239−1254.
(29) Wang, Y.; Xiao, J.; Suzek, T. O.; Zhang, J.; Wang, J.; Zhou, Z.; Han, L.; Karapetyan, K.; Dracheva, S.; Shoemaker, B. A.; et al. PubChem's BioAssay Database. *Nucleic Acids Res.* **2012**, *40* (D1), D400−412.
(30) Yu, Y.; Zhou, M.; Long, X.; Yin, S.; Hu, G.; Yang, X.; Jian, W.; Yu, R. Study on the mechanism of action of colchicine in the treatment of coronary artery disease based on network pharmacology and molecular docking technology. *Front. Pharmacol.* **2023**, *14*, No. 1147360.
(31) Davis, A. P.; Wiegers, T. C.; Johnson, R. J.; Sciaky, D.; Wiegers, J.; Mattingly, C. J. Comparative Toxicogenomics Database (CTD): update 2023. *Nucleic Acids Res.* **2023**, *51* (D1), D1257−D1262.
(32) Bateman, A.; Martin, M. J.; Orchard, S.; et al. UniProt: the Universal Protein Knowledgebase in 2023. *Nucleic Acids Res.* **2023**, *51* (D1), D523−D531.
(33) Rebhan, M.; Chalifa-Caspi, V.; Prilusky, J.; Lancet, D. GeneCards: integrating information about genes, proteins and diseases. *Trends Genet.* **1997**, *13* (4), 163.
(34) Amberger, J. S.; Bocchini, C. A.; Schiettecatte, F.; Scott, A. F.; Hamosh, A. OMIM.org: Online Mendelian Inheritance in Man, an online catalog of human genes and genetic disorders. *Nucleic Acids Res.* **2015**, *43* (D1), D789−D798.
(35) Barbarino, J. M.; Whirl-Carrillo, M.; Altman, R. B.; Klein, T. E. PharmGKB: A worldwide resource for pharmacogenomic information. *Wiley Interdiscip. Rev.: Syst. Biol. Med.* **2018**, *10* (4), No. e1417.
(36) Deng, W.; Huang, Y.; Li, H.; Chen, C.; Lin, Y.; Wang, M.; Huang, H.; Liu, T.; Qin, Q.; Shao, Y.; et al. Dehydromiltirone inhibits osteoclast differentiation in RAW264.7 and bone marrow macrophages by modulating MAPK and NF-κB activity. *Front. Pharmacol.* **2022**, *13*, No. 1015693.
(37) Szklarczyk, D.; Kirsch, R.; Koutrouli, M.; Nastou, K.; Mehryary, F.; Hachilif, R.; Gable, A. L.; Fang, T.; Doncheva, N. T.; Pyysalo, S.; et al. The STRING database in 2023: protein-protein association networks and functional enrichment analyses for any sequenced genome of interest. *Nucleic Acids Res.* **2023**, *51* (D1), D638−D646.
(38) Majeed, A.; Mukhtar, S. Protein-Protein Interaction Network Exploration Using Cytoscape. *Methods Mol. Biol.* **2023**, *2690*, 419−427.
(39) Chin, C. H.; Chen, S. H.; Wu, H. H.; Ho, C. W.; Ko, M. T.; Lin, C. Y. cytoHubba: identifying hub objects and sub-networks from complex interactome. *BMC Syst. Biol.* **2014**, *8* (Suppl 4), No. S11.
(40) Chen, L.; Zhang, Y. H.; Wang, S.; Zhang, Y.; Huang, T.; Cai, Y. D. Prediction and analysis of essential genes using the enrichments of gene ontology and KEGG pathways. *PLoS One* **2017**, *12* (9), No. e0184129.
(41) Huang, D. W.; Sherman, B. T.; Lempicki, R. A. Systematic and integrative analysis of large gene lists using DAVID bioinformatics resources. *Nat. Protoc.* **2009**, *4* (1), 44−57.
(42) Seeliger, D.; de Groot, B. L. Ligand docking and binding site analysis with PyMOL and Autodock/Vina. *J. Comput.-Aided Mol. Des.* **2010**, *24* (5), 417−422.
(43) Kuan, F. C.; Li, J. M.; Huang, Y. C.; Chang, S. F.; Shi, C. S. Therapeutic Potential of Regorafenib in Cisplatin-Resistant Bladder Cancer with High Epithelial-Mesenchymal Transition and Stemness Properties. *Int. J. Mol. Sci.* **2023**, *24* (24), 17610.
(44) Collin-Osdoby, P.; Osdoby, P. RANKL-mediated osteoclast formation from murine RAW 264.7 cells. *Methods Mol. Biol.* **2012**, *816*, 187−202.
(45) Wilhelm, S. M.; Dumas, J.; Adnane, L.; Lynch, M.; Carter, C. A.; Schütz, G.; Thierauch, K. H.; Zopf, D. Regorafenib (BAY 73−4506): a new oral multikinase inhibitor of angiogenic, stromal and oncogenic receptor tyrosine kinases with potent preclinical antitumor activity. *Int. J. Cancer* **2011**, *129* (1), 245−255.
(46) Liu, C.; Zhao, M.; Chen, J.; Xu, L.; Wang, K.; Li, G. Nodakenin alleviates ovariectomy-induced osteoporosis by modulating osteoblastogenesis and osteoclastogenesis. *Eur. J. Pharmacol.* **2023**, *960*, No. 176121.
(47) Mao, Y.; Xie, X.; Jiang, T.; Chao, R.; Wan, T.; Sun, L.; Sun, G.; Zhou, Z.; Xu, W.; Chen, X.; Zhang, S. Xl019, a novel JAK inhibitor, suppressed osteoclasts differentiation induced by RANKL through MAPK signaling pathway. *Biochem. Pharmacol.* **2023**, *215*, No. 115704.
(48) Ou, D. L.; Chen, C. W.; Hsu, C. L.; Chung, C. H.; Feng, Z. R.; Lee, B. S.; Cheng, A. L.; Yang, M. H.; Hsu, C. Regorafenib enhances antitumor immunity via inhibition of p38 kinase/Creb1/Klf4 axis in tumor-associated macrophages. *J. Immunother. Cancer* **2021**, *9* (3), No. e001657.
(49) Park, J. J.; Oh, K.; Lee, G. W.; Bang, G.; Park, J. H.; Kim, H. B.; Kim, J. Y.; Shin, E. Y.; Kim, E. G. Defining regorafenib as a senomorphic drug: therapeutic potential in the age-related lung disease emphysema. *Exp. Mol. Med.* **2023**, *55* (4), 794−805.
(50) Ihn, H. J.; Kim, T. H.; Kim, K.; Kim, G. Y.; Jeon, Y. J.; Choi, Y. H.; Bae, J. S.; Kim, J. E.; Park, E. K. 2-O-digalloyl-1,3,4,6-tetra-O-galloyl-β-D-glucose isolated from Galla Rhois suppresses osteoclast differentiation and function by inhibiting NF-κB signaling. *BMB Rep.* **2019**, *52* (6), 409−414.
(51) Chen, K.; Yuan, Y.; Wang, Z.; Song, D.; Zhao, J.; Cao, Z.; Chen, J.; Guo, Q.; Chen, L.; Tickner, J.; Xu, J. Helvolic acid attenuates osteoclast formation and function via suppressing RANKL-induced NFATc1 activation. *J. Cell. Physiol.* **2019**, *234* (5), 6477−6488.
(52) Yasuda, H. Discovery of the RANKL/RANK/OPG system. *J. Bone Miner. Metab.* **2021**, *39* (1), 2−11.
(53) Oh, K.; Lee, G. W.; Kim, H. B.; Park, J. H.; Shin, E. Y.; Kim, E. G. Regorafenib prevents the development of emphysema in a murine elastase model. *BMB Rep.* **2023**, *56* (8), 439−444.
(54) Veeroju, S.; Kojonazarov, B.; Weiss, A.; Ghofrani, H. A.; Weissmann, N.; Grimminger, F.; Seeger, W.; Novoyatleva, T.; Schermuly, R. T. Therapeutic Potential of Regorafenib-A Multikinase Inhibitor in Pulmonary Hypertension. *Int. J. Mol. Sci.* **2021**, *22* (3), 1502.
(55) Markovics, A.; Toth, D. M.; Glant, T. T.; Mikecz, K. Regulation of autoimmune arthritis by the SHP-1 tyrosine phosphatase. *Arthritis Res. Ther* **2020**, *22* (1), 160.
(56) Han, K. M.; Kang, R. J.; Jeon, H.; Lee, H. J.; Lee, J. S.; Park, H.; Gak Jeon, S.; Suk, K.; Seo, J.; Hoe, H. S. Regorafenib Regulates AD Pathology, Neuroinflammation, and Dendritic Spinogenesis in Cells and a Mouse Model of AD. *Cells* **2020**, *9* (7), 1655.
(57) Min, H. K.; Kim, S. H.; Won, J. Y.; Kim, K. W.; Lee, J. Y.; Lee, S. H.; Kim, H. R. Dasatinib, a selective tyrosine kinase inhibitor, prevents joint destruction in rheumatoid arthritis animal model. *Int. J. Rheum. Dis.* **2023**, *26* (4), 718−726.
(58) Heilmann, T.; Rumpf, A. L.; Roscher, M.; Tietgen, M.; Will, O.; Gerle, M.; Damm, T.; Borzikowsky, C.; Maass, N.; Glüer, C. C.; et al. Dasatinib prevents skeletal metastasis of osteotropic MDA-MB-231 cells in a xenograft mouse model. *Arch. Gynecol. Obstet.* **2020**, *301* (6), 1493−1502.
(59) Kim, H. J.; Yoon, H. J.; Choi, J. Y.; Lee, I. K.; Kim, S. Y. The tyrosine kinase inhibitor GNF-2 suppresses osteoclast formation and activity. *J. Leukocyte Biol.* **2013**, *95* (2), 337−345.

https://doi.org/10.1021/acsomega.4c01308
ACS Omega 2024, 9, 33574−33593

(60) Nogales, C.; Mamdouh, Z. M.; List, M.; Kiel, C.; Casas, A. I.; Schmidt, H. Network pharmacology: curing causal mechanisms instead of treating symptoms. *Trends Pharmacol. Sci.* **2022**, *43* (2), 136−150.
(61) Hopkins, A. L. Network pharmacology: the next paradigm in drug discovery. *Nat. Chem. Biol.* **2008**, *4* (11), 682−690.
(62) Tang, L.; Wu, M.; Lu, S.; Zhang, H.; Shen, Y.; Shen, C.; Liang, H.; Ge, H.; Ding, X.; Wang, Z. Fgf9 Negatively Regulates Bone Mass by Inhibiting Osteogenesis and Promoting Osteoclastogenesis Via MAPK and PI3K/AKT Signaling. *J. Bone Miner. Res.: Off. J. Am. Soc. Bone Miner. Res.* **2020**, *36* (4), 779−791.
(63) Jiang, T.; Gong, Y.; Zhang, W.; Qiu, J.; Zheng, X.; Li, Z.; Yang, G.; Hong, Z. PD0325901, an ERK inhibitor, attenuates RANKL-induced osteoclast formation and mitigates cartilage inflammation by inhibiting the NF-κB and MAPK pathways. *Bioorg. Chem.* **2023**, *132*, No. 106321.
(64) Liu, C.-L.; Ho, T.-L.; Fang, S.-Y.; Guo, J.-H.; Wu, C.-Y.; Fong, Y.-C.; Liaw, C.-C.; Tang, C.-H. Ugonin L inhibits osteoclast formation and promotes osteoclast apoptosis by inhibiting the MAPK and NF-κB pathways. *Biomed. Pharmacother.* **2023**, *166*, No. 115392.
(65) Asl, E. R.; Amini, M.; Najafi, S.; Mansoori, B.; Mokhtarzadeh, A.; Mohammadi, A.; Lotfinejad, P.; Bagheri, M.; Shirjang, S.; Lotfi, Z.; et al. Interplay between MAPK/ERK signaling pathway and MicroRNAs: A crucial mechanism regulating cancer cell metabolism and tumor progression. *Life Sci.* **2021**, *278*, No. 119499.
(66) Udagawa, N.; Koide, M.; Nakamura, M.; Nakamichi, Y.; Yamashita, T.; Uehara, S.; Kobayashi, Y.; Furuya, Y.; Yasuda, H.; Fukuda, C.; Tsuda, E. Osteoclast differentiation by RANKL and OPG signaling pathways. *J. Bone Miner. Metab.* **2021**, *39* (1), 19−26.
(67) Guo, J.; Ren, R.; Sun, K.; Yao, X.; Lin, J.; Wang, G.; Guo, Z.; Xu, T.; Guo, F. PERK controls bone homeostasis through the regulation of osteoclast differentiation and function. *Cell Death Dis.* **2020**, *11* (10), 847.
(68) Ding, D.; Yan, J.; Feng, G.; Zhou, Y.; Ma, L.; Jin, Q. Dihydroartemisinin attenuates osteoclast formation and bone resorption via inhibiting the NF-κB, MAPK and NFATc1 signaling pathways and alleviates osteoarthritis. *Int. J. Mol. Med.* **2021**, *49* (1), 4.
(69) Qiu, J.; Jiang, T.; Yang, G.; Gong, Y.; Zhang, W.; Zheng, X.; Hong, Z.; Chen, H. Neratinib exerts dual effects on cartilage degradation and osteoclast production in Osteoarthritis by inhibiting the activation of the MAPK/NF-κB signaling pathways. *Biochem. Pharmacol.* **2022**, *205*, No. 115155.
(70) Cong, Q.; Jia, H.; Li, P.; Qiu, S.; Yeh, J.; Wang, Y.; Zhang, Z. L.; Ao, J.; Li, B.; Liu, H. p38α MAPK regulates proliferation and differentiation of osteoclast progenitors and bone remodeling in an aging-dependent manner. *Sci. Rep.* **2017**, *7*, No. 45964.
(71) Sheng, S. R.; Wu, Y. H.; Dai, Z. H.; Jin, C.; He, G. L.; Jin, S. Q.; Zhao, B. Y.; Zhou, X.; Xie, C. L.; Zheng, G.; Tian, N. F. Safranal inhibits estrogen-deficiency osteoporosis by targeting Sirt1 to interfere with NF-κB acetylation. *Phytomedicine* **2023**, *114*, No. 154739.
(72) Ding, P.; Gao, C.; Gao, Y.; Liu, D.; Li, H.; Xu, J.; Chen, X.; Huang, Y.; Zhang, C.; Zheng, M.; Gao, J. Osteocytes regulate senescence of bone and bone marrow. *eLife* **2022**, *11*, No. e81480.
(73) Wang, T.; Liu, Q.; Tjhioe, W.; Zhao, J.; Lu, A.; Zhang, G.; Tan, R. X.; Zhou, M.; Xu, J.; Feng, H. T. Therapeutic Potential and Outlook of Alternative Medicine for Osteoporosis. *Curr. Drug Targets* **2017**, *18* (9), 1051−1068.
(74) He, J.; Li, X.; Wang, Z.; Bennett, S.; Chen, K.; Xiao, Z.; Zhan, J.; Chen, S.; Hou, Y.; Chen, J.; et al. Therapeutic Anabolic and Anticatabolic Benefits of Natural Chinese Medicines for the Treatment of Osteoporosis. *Front. Pharmacol.* **2019**, *10*, 1344.
(75) Garcia-Gomez, A.; Ocio, E. M.; Crusoe, E.; Santamaria, C.; Hernández-Campo, P.; Blanco, J. F.; Sanchez-Guijo, F. M.; Hernández-Iglesias, T.; Briñón, J. G.; Fisac-Herrero, R. M.; et al. Dasatinib as a bone-modifying agent: anabolic and anti-resorptive effects. *PLoS One* **2012**, *7* (4), No. e34914.
(76) Kroschwald, L. M.; Tauer, J. T.; Kroschwald, S. I.; Suttorp, M.; Wiedenfeld, A.; Beissert, S.; Bauer, A.; Rauner, M. Imatinib mesylate and nilotinib decrease synthesis of bone matrix in vitro. *Oncol. Lett.* **2019**, *18* (2), 2102−2108.

https://doi.org/10.1021/acsomega.4c01308
ACS Omega 2024, 9, 33574−33593